NASA

Technical Memorandum 84927

A Statistical Examination of Nimbus 7 SMMR Data and Remote Sensing of Sea Surface Temperature, Liquid Water Content in the Atmosphere and Surfaces Wind Speed

C. Prabhakara, I. Wang, A.T.C. Chang, P. Gloersen

OCTOBER 1982

National Aeronautics and Space Administration

Goddard Space Flight Center
Greenbelt, Maryland 20771

A STATISTICAL EXAMINATION OF NIMBUS 7 SMMR DATA AND REMOTE SENSING OF SEA SURFACE TEMPERATURE, LIQUID WATER CONTENT IN THE ATMOSPHERE AND SURFACES WIND SPEED

C. Prabhakara,

I. Wang**,

A. T. C. Chang*,

P. Gloersen

Laboratory for Atmospheric Sciences,
NASA/GODDARD SPACE FLIGHT CENTER
Greenbelt, Maryland 20771

October 1982

* Earth Survey Applications Division, NASA/GSFC

** Computer Sciences Corporation, Silver Spring, Maryland 20910

ABSTRACT

Nimbus 7 Scanning Multichannel Microwave Radiometer (SMMR) brightness temperature measurements over the global oceans have been examined with the help of statistical and empirical techniques. Such analyses show that zonal averages of brightness temperature measured by SMMR, over the oceans, on a large scale are primarily influenced by the water vapor in the atmosphere. Liquid water in the clouds and rain, which has a much smaller spatial and temporal scale, contributes substantially to the variability of the SMMR measurements within the latitudinal zones. The surface wind not only increases the surface emissivity but through its interactions with the atmosphere produces correlations, in the SMMR brightness temperature data, that have significant meteorological implications. It is found that a simple meteorological model can explain the general characteristics of the SMMR data. With the help of this model methods to infer, over the global oceans, the surface temperature, liquid water content in the atmosphere, and surface wind speed are developed. Monthly mean estimates of the sea surface temperature and surface winds are compared with the ship measurements. Estimates of liquid water content in the atmosphere are consistent with earlier satellite measurements.

A STATISTICAL EXAMINATION OF NIMBUS 7 SMMR DATA AND REMOTE SENSING OF SEA SURFACE TEMPERATURE, LIQUID WATER CONTENT IN THE ATMOSPHERE AND SURFACES WIND SPEED

INTRODUCTION

The Scanning Multichannel Microwave Radiometer (SMMR) is designed with the objective to map, over the open ocean, sea surface temperature (SST), surface wind speed, atmospheric integrated water vapor content, integrated liquid water content, and rainfall, and to determine sea-ice type and extent (Gloersen and Barath, 1977). SMMR was flown on Seasat and Nimbus 7 that were launched in 1978. The SMMR on Seasat gathered data for 3 months, from July to October of 1978 when that satellite stopped functioning. The Nimbus 7 SMMR has been gathering data from October 1978 to the present time, giving us a long record of data that could be useful for climatological investigations. In this study we have made an attempt to derive monthly mean sea surface temperature, liquid water content in the atmosphere and the surface wind speed from Nimbus 7 SMMR data for two 30 day periods, Oct. 25-Nov. 25, 1978 and Feb. 15-Mar. 15, 1979. The retrieval of water vapor information for these periods from Nimbus 7 SMMR data was reported in an earlier study (Prabhakara et al. 1982). The techniques developed in these two studies could be applied to the long record of Nimbus 7 SMMR measurements to derive climatology on four of the parameters stated in the objective.

SMMR is a five-channel radiometer that measures the earth's brightness temperature at 6.6, 10.7, 18, 21 and 37 GHz in dual polarization. The conical scanning geometry of SMMR is such that the instrument views the earth's surface at a constant incidence angle of about 50°. The spatial resolution of the instrument is proportional to the wave length and varies from about 155 km at 6.6 GHz to about 30 km at 37 GHz. Gloersen and Hardis (1978) have presented a description of Nimbus 7 SMMR and the calibration method to arrive at brightness temperature measurements.

Absolute calibration of the SMMR data involves careful treatment of the antenna sidelobe contribution and polarization cross coupling (see for Eg. Njoku, 1980). In practice residual errors of systematic type remain in the data after calibration. For this reason in this study a remote sensing scheme is developed that does not depend critically on the absolute brightness temperature values but on their spatial and temporal changes.

The ability of the passive microwave technique to sense the sea surface temperature through light non-raining clouds is valuable in generating this information on a global basis. Inference of the surface wind speed and liquid water content in the atmosphere over the global oceans can aid studies involving air sea interactions. This investigation demonstrates the feasibility of getting this information on a monthly mean basis from microwave remote sensing.

Theoretical Background

In the microwave spectral region between 6.6 to 37 GHz a weak water vapor line is present with its center at 22.235 GHz. As water vapor is a common constituent of the atmosphere, brightness temperature measurements made by SMMR reveal this water vapor line globally. Further this line shows up in a pronounced way in the water-vapor-rich tropics and somewhat weakly in the high latitudes where water vapor is less aboundant. Liquid droplets in the clouds and rain absorb and scatter microwave radiation. Clouds and rain are generally limited in geographical extent and in such regions the microwave brightness temperatures are significantly modulated by the liquid water in the atmosphere. The sea surface emissivity in this spectral region increases as a function of the frequency and in the absence of surface winds depends mainly on the sea surface temperature. The wind at the sea surface changes the roughness of the water and thereby the surface emissivity, and in addition at wind speeds above about 10 m/s white caps are formed which markedly affect the sea surface emissivity. These physical effects have been discussed in earlier studies among others by Wilheit and Chang (1980), Wilheit (1978),

Chang and Wilheit (1979), Staelin et al. (1976), and Swift (1980). In this study the existing framework of physics is adopted and applied to the Nimbus 7 SMMR data to retrieve the various geophysical informations mentioned above.

The radiative transfer scheme elaborated by Chang and Wilheit (1979) is adopted in this study. The emissivity of the smooth sea surface is calculated from the dielectric constant using the Fresnel relations (Jackson, 1962). The dielectric constant data of Lane and Saxton (1952) are used in these calculations. Since the dielectric constant is a function of wavelength of radiation and the temperature of the water, the microwave emissivity changes as a function of these variables as shown in Figure 1. The emissivity of the sea surface in the vertical and horizontal polarizations applicable to SMMR channels at 50° incidence angle is shown. It may be noted that at 6.6 GHz the sea surface emissivity from about 273°K to 303°K, covering essentially the range of sea surface temperatures, is nearly constant. At the higher frequencies a negative temperature dependence that increases with the frequency is noticed. Liquid water droplets, as stated earlier, in the clouds and rain absorb and scatter microwave radiation. As long as $\lambda \gg D$, where λ is the wavelength of radiation and D the diameter of a droplet, is satisfied the Rayleigh approximation may be adopted (Gunn and East, 1954; Tsang et al, 1977) and the absorption by the droplets is nearly equal to the extinction. Using this approximation together with the frequency dependence of the dielectric constant one finds the absorption due to water droplets increases nearly as a square of the frequency with a significant negative dependence on the temperature of the drops as shown in Figure 2 (see Wilheit and Chang, 1980).

The emissivity of the smooth sea surface in the microwave region is a function of the viewing angle and polarization. Utilizing the geometric optics, and Cox and Munk's (1955) expressions for the variance of the sea surface slopes as a function of the surface wind speed, one can derive the change in the surface emissivity due to wind (Wilheit, 1979). In addition at wind speeds above about 10 m/s foam cover on sea water starts to increase significantly the

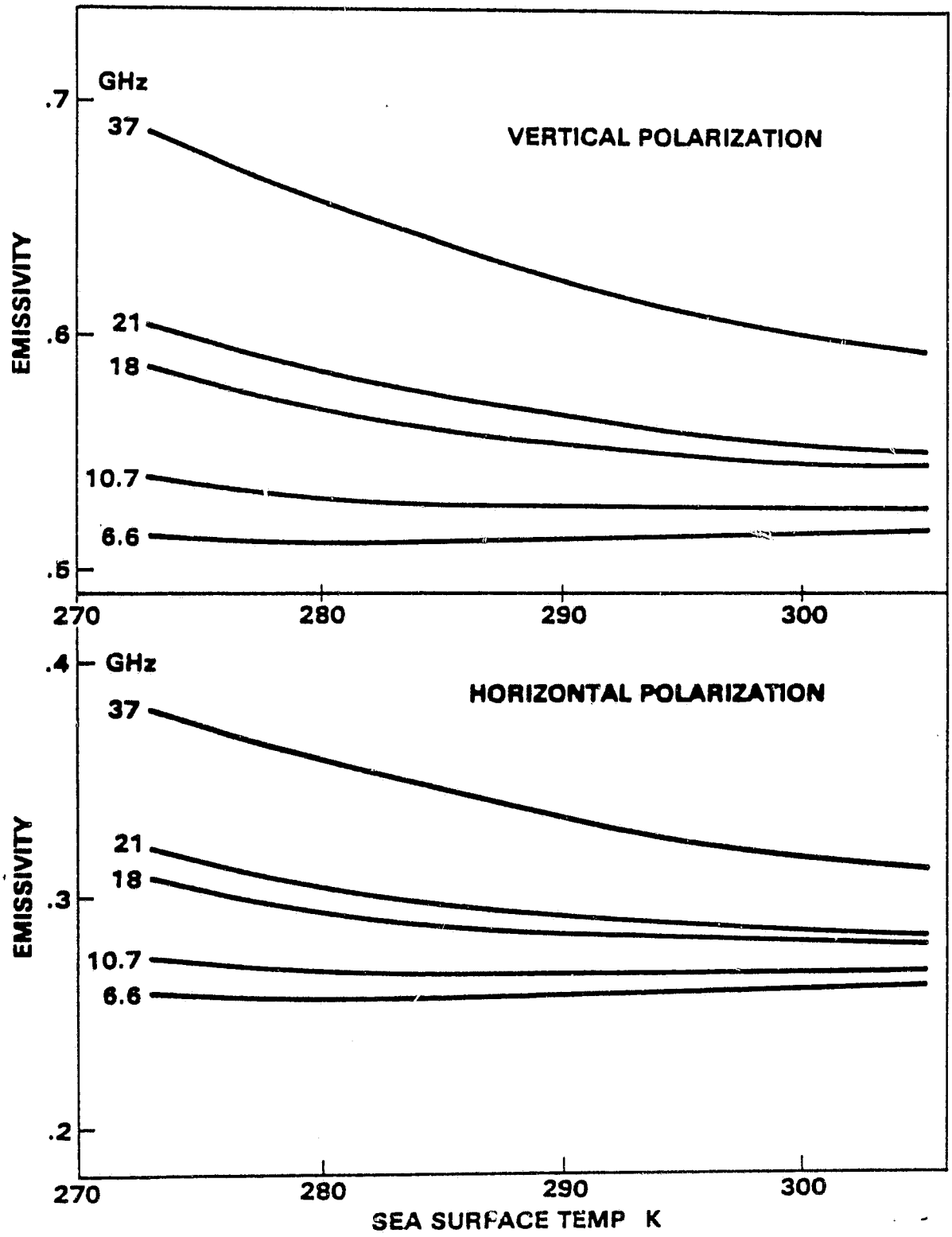

Figure 1. Variation of smooth sea surface emissivity as a function of temperature for SMMR frequencies at incidence angle of 50°.

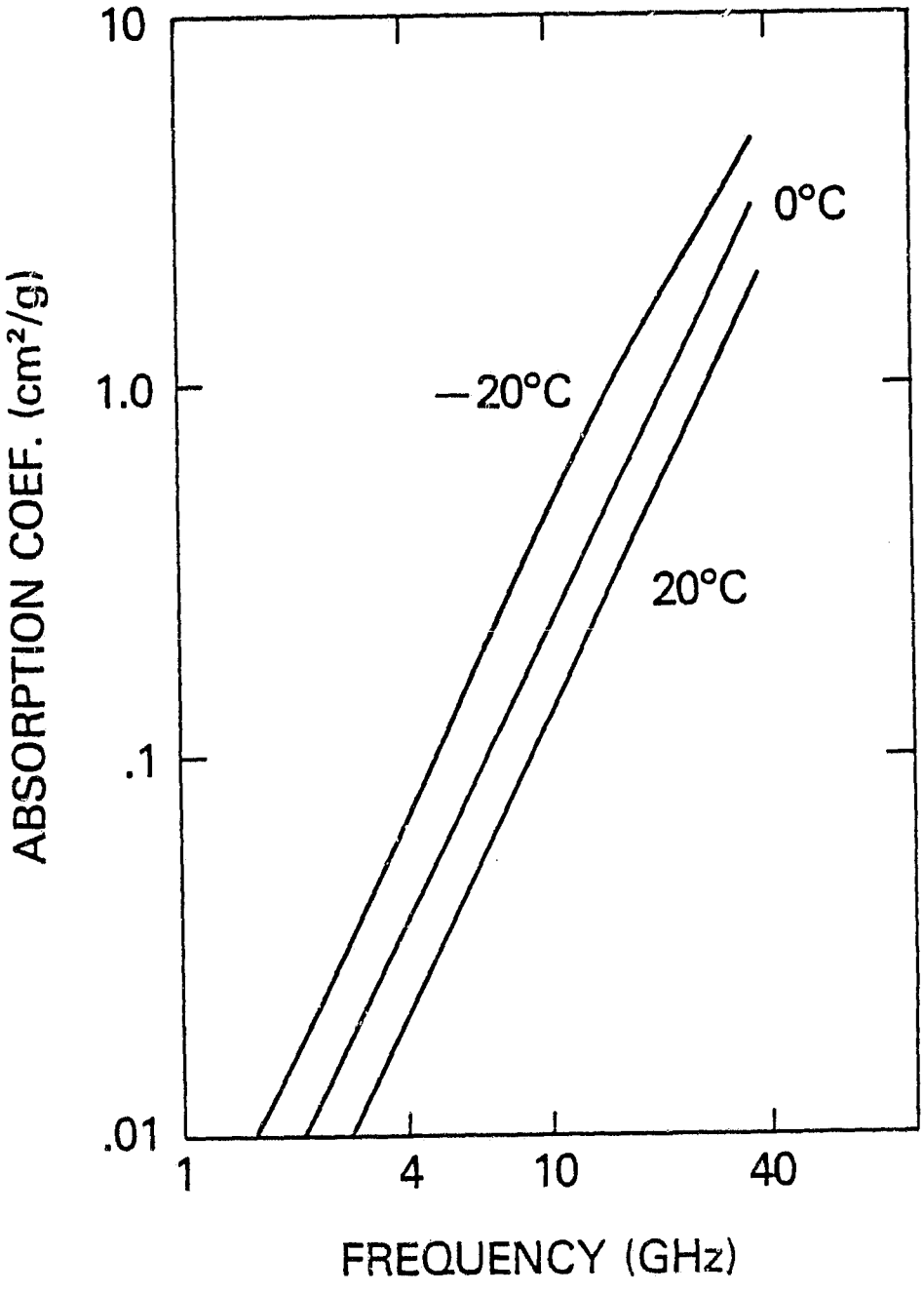

Figure 2. Microwave absorption coefficient for liquid water droplets as a function of frequency and temperature.

sea surface emissivity (Nordberg et al., 1971; Webster et al., 1976). It is, therefore, helpful to have a simple model of the sea surface emissivity as a function of wind speed that includes the effects of surface roughness and foam. Such a model is empirically derived by Wentz (1981) utilizing the simultaneous measurements made by Seasat SMMR and SASS (Seasat-A Scatterometer) that were flown on the same satellite.

In order to complete the picture the water vapor absorption spectrum in the 6 to 37 GHz region, applicable at sea level pressure, is presented in Figure 3. The presence of water vapor and hence its absorption in the microwave region, over the global oceans cannot be ignored in retreiving other geophysical parameters.

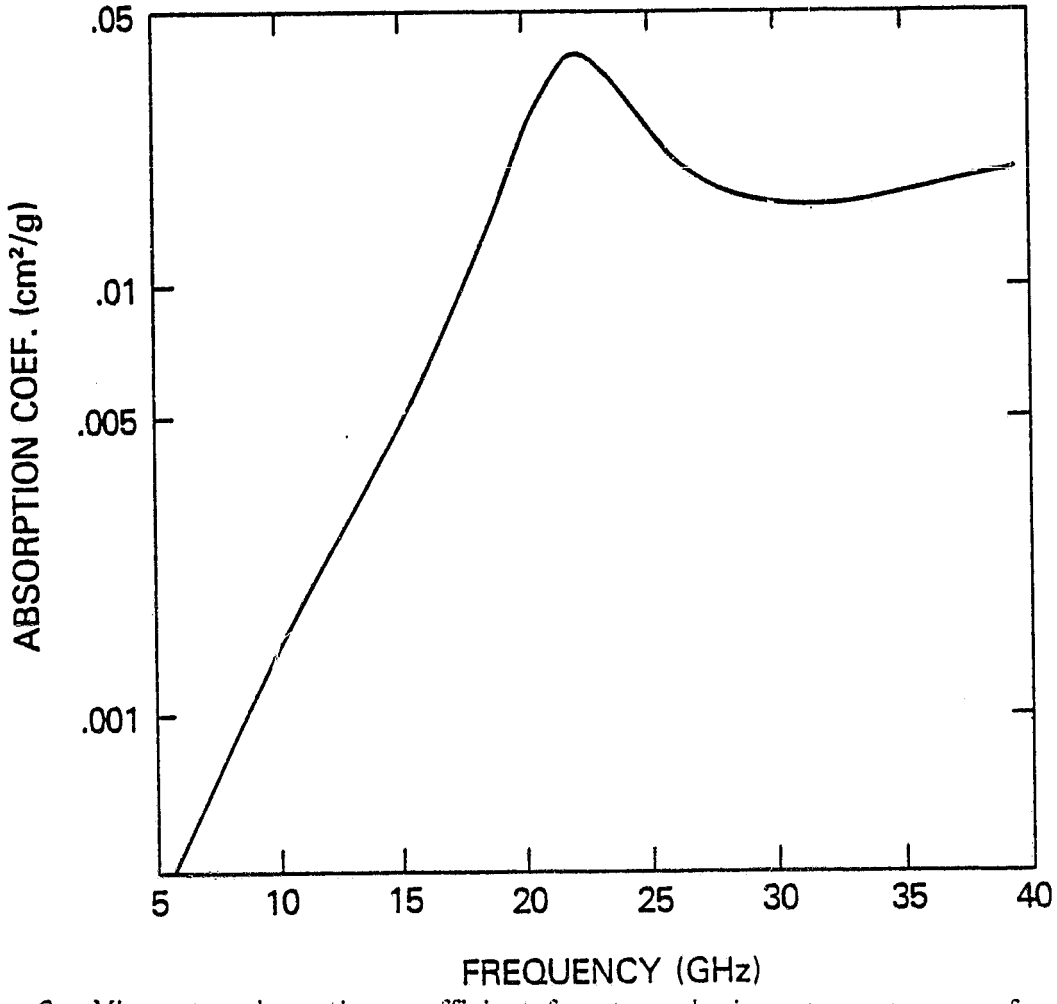

Figure 3. Microwave absorption coefficient for atmospheric water vapor as a function of frequency at sea level pressure.

The radiative transfer equation in the microwave region can be written as

$$T_{B_\nu} = T_S \epsilon_\nu \tau_{o_\nu} + \int_{\tau_{o_\nu}}^{1} T(P)\, d\, \tau_\nu\,(P) + R_\nu \tau_{o_\nu} \int_{\tau_{o_\nu}}^{1} T(P)\, d\, \tau_\nu^{1}\,(P) \qquad (1)$$

where ν is the frequency, T_{B_ν}, the brightness temperature at the top of the atmosphere measured by the satellite sensor, P the pressure, T_S and T(P) are the temperature at surface and at pressure level P, respectively. τ_{o_ν} and $\tau_\nu(P)$ are the transmission of the atmosphere from the surface and from any pressure level P to the satellite respectively. $\tau_\nu^{1}(P)$ is the transmission of the atmosphere from any pressure level P to the surface. ϵ_ν is the surface emissivity and R_ν the reflectivity of the surface. Furthermore $\epsilon_\nu + R_\nu = 1$.

Since the line of sight from SMMR to the earth makes an angle of 50° with respect to the local vertical at the surface, all the quantities τ_{o_ν}, τ_ν, τ_ν^{1}, ϵ_ν and R_ν are calculated along that direction.

The first term in the transfer equation represents the surface emission, the second term the atmospheric emission, and the third term corresponds to the atmospheric radiation reflected at the surface and then transmitted to the satellite sensor. The sea surface acts like a specular reflector under calm conditions. Equation (1) thus holds good for specular reflection. One may choose to include the effects of non-specular reflection, induced by the wind at the surface, in the radiative transfer equation (see e.g. Wentz, 1981). Such non-specular effects are of second order in magnitude. As such equation (1) is an approximation to the radiative transfer when the sea surface is disturbed.

In order to appreciate the salient aspects of the physics contained in equation (1) we can approximate the two integrals as follows

$$\int_{\tau_{o_\nu}}^{1} T(P)\, d\, \tau_\nu\,(P) \cong \overline{T}_\nu\,(1 - \tau_{o_\nu}) \qquad (2)$$

and

$$\int_{\tau_{o_\nu}}^{1} T(P)\, d\, \tau_\nu^{\uparrow}(P) \cong \bar{T}_\nu^{\uparrow} (1 - \tau_{o_\nu}) \tag{3}$$

where $\bar{T}_\nu$ is the equivalent radiative temperature of the atmosphere for the upwelling radiation, while $\bar{T}_\nu^{\downarrow}$ corresponds to that of the downwelling radiation. Furthermore as τ is heavily weighted towards the lowest layers in the atmosphere, we can assume $\bar{T}_\nu \cong \bar{T}_\nu^{\downarrow} \cong T_S$.

With the above simplifications equation (1) may be written as

$$T_{B_\nu} \cong T_S \left[1 - \tau_{o_\nu}^2 (1 - \epsilon_\nu)\right] \tag{4}$$

Differentiating eq. (4) with respect to frequency, we get

$$\partial T_{B_\nu}/\partial\nu \cong - T_S \frac{\partial}{\partial\nu} \underbrace{\left[\tau_{o_\nu}^2 \ (1 - \epsilon_\nu)\right]}_{(a)} \tag{5}$$

Equation (5) states in a simple way that spectral changes in brightness temperature are related to the spectral changes in the product quantity (a) contained in equation (5). This renders the problem of determining τ_{o_ν} or ϵ_ν from multispectral measurements a non-linear one.

When ϵ_ν is nearly constant, say $\tilde{\epsilon}$, in a small spectral interval $\partial\nu$, equation (5) may be approximated further as

$$\partial T_{B_\nu}/\partial\nu \cong - T_S (1 - \tilde{\epsilon})\, \partial\tau_{o_\nu}^2/\partial\nu \tag{6}$$

The method developed by Prabhakara et al., (1982) to determine water vapor amount w in the atmosphere, using 18 and 21 GHz SMMR measurements, was based on this principle. The surface temperature T_S, surface wind speed u and total liquid droplet content ℓ are not readily derivable from simple considerations such as those represented by eq. (6) because of the non-linearities.

In order to retrieve the various geophysical parameters Wilheit and Chang (1980) have developed a multiple linear regression scheme. Wentz (1982) has devised a least squares method to do the same. These retrieval schemes amount to taking SMMR measurements at various frequencies in dual polarization at a given location at one instant and invert them to retrieve geophysical parameters. As will be shown in the following sections, the method developed in this study differs in this respect.

Generally the retrieval schemes inherently take into account the sensitivity of the brightness temperatures to the various geophysical parameters. These sensitivities are determined theoretically from radiative transfer calculations. In Table 1 typical sensitivity of each SMMR channel to the parameters T_S, w, ℓ and u is presented. These sensitivities for T_S, w and ℓ are derived from equation (1) for a tropical model atmosphere containing 3.4 g/cm^2 of water vapor, 50 mg/cm^2 of liquid droplets, surface temperature of 298.6 K and no wind at the surface. The sensitivity to the surface wind speed shown in Table 1 is based on the observations of Webster et al., (1976) when the wind speed exceeds ~ 10 m/s. Sensitivity below that speed is considerably weak.

From Table 1 we see the 6.6 and 10.7 GHz channels depend weakly on the absorption due to water vapor and liquid water. Hence these channels are called surface channels, while 18, 21 and 37 GHz channels that are affected by the atmospheric constituents are called the atmospheric channels.

In principle the sensitivities given in Table 1 constitute the coefficients of a linear set of algebraic equations to solve for the unknown magnitude of the geophysical parameters. Different techniques exist to invert such a system of equations in a linear way or through iterative schemes in a non-linear manner. However, in practice calibration biases, i.e. systematic offsets, sometimes can cause considerable difficulty in getting satisfactory solutions. This is particularly

Table 1. Sensitivity of SMMR brightness temperatures T_B.

	SURFACE CHANNELS				ATMOSPHERIC CHANNELS					
ν(GHz)	6.6		10.7		18		21		37	
POLARIZATION	V	H	V	H	V	H	V	H	V	H
$\frac{\partial T_B}{\partial T_S}$ (K/K)	0.5	0.3	0.5	0.3	0.3	0.2	0.2	0.1	0.1	-0.1
$\frac{\partial T_B}{\partial w}$ ($K/g/cm^2$)	0.3	0.5	0.8	1.3	4.5	7.5	11.9	19.6	6	11
$\frac{\partial T_B}{\partial \ell}$ ($K/10^{-2}g/cm^2$)	0.3	0.5	0.7	1.1	1.6	2.7	1.5	2.5	4.2	7.8
$\frac{\partial T_B}{\partial \mu}$ ($K/m/s$)	~0.5	~1.0	~0.5	~1.0	~0.5	~1.0	~0.5	~1.0	~0.5	~1.0

T_S – Sea surface temp (°C)

w – total water vapor in the atmosphere (g/cm^2)

ℓ – total liquid water content in the atmosphere (10^{-2} g/cm^2)

u – surface wind speed (m/s)

so in the case of SMMR where the systematic offsets differ from channel to channel, between night and day, and as a function of cross track scan position. Slow degradation of the sensors in time is another possible systematic problem. It may be possible to correct the data for some of these systematic offsets with the help of ground truth. Hoffer et al. (1980) and Wentz et al. (1982) followed such a procedure to retrieve information from Seasat SMMR data. Generally such a procedure limits the data analysis to some time interval and/or geographical area.

Somewhat different approach is taken in this study to retrieve information from Nimbus 7 SMMR data on a monthly mean basis over global oceans. This approach is developed after some detailed examination of the data that is presented in the next section.

After such an examination it is found that one simple adjustment, namely a constant shift in the 6.6 GHz brightness temperature, is necessary to account for calibration error. With the corrected 6.6 GHz data one can estimate the sea surface temperature globally. Futher it is observed that the temporal variation in the brightness temperatures, at each location on the global oceans, can be assessed in an objective fashion nearly independent of calibration offsets. From such temporal variations information about liquid water in the atmosphere and surface wind speed can be determined.

At this point it is necessary to discuss the relative merits of the vertical vs horizontal polarization data for the determination of surface wind and surface temperature which produce relatively small change in the microwave brightnesses (see Table 1). First of all the brightness temperature in the horizontal is about half as much as that in the vertical. So for a given instrument noise equivalent temperature (NEΔT) the horizontal data will be poor as compared to the vertical. Secondly, from the sensitivity considerations we see for the sea surface temperature determination the vertical polarization data in the 6.6 GHz is preferable. For these two reasons the vertical polarization data are preferred in this analysis for sea surface temperature

estimation and surface wind inference. The atmospheric variables, on the other hand, produce substantial change in the microwave brightness in both polarizations and preference for particular polarization is not critical for their determination. Based on this reasoning the rest of the analysis presented in this study is focussed on vertical polarization data.

Statistical Examination of the SMMR Data:

The Nimbus 7 SMMR brightness temperature data used in this study have a 155 km field of view or cell size (Gloersen and Hardis, 1978) at the earth's surface. In order to minimize errors due to calibration, SMMR data along the subsatellite track and observed during descending node, i.e. night time data, are subjected to statistical analysis.

The latitudinal mean and standard deviation of SMMR data chosen in the above manner, over the oceans, are calculated from the equator to high latitudes. In Figure 4 the spectra of the mean and standard deviation of the vertical polarization data at several latitudes is shown. The mean clearly shows the water vapor line at all latitudes and to a first approximation the strength of this line indicates the latitudinal variation of water vapor amount in the atmosphere. Notice the maximum in line strength occurs at 7°N where the Intertropical Convergence Zone, ITCZ, is present. It is known from earlier investigations (Grody et al., 1980; Prabhakara et al., 1982) that the maximum in water vapor occurs near ITCZ. The influence of liquid water present in the clouds and rain does not seem to have a dominant influence on the mean spectra.

The spectra of the standard deviation show somewhat different information. The lack of organized change, with latitude, in these spectra is apparent. At 7°N, near ITCZ, the standard deviation at 21 GHz is smaller than that at 18 GHz. This behavior has been simulated in our theoretical calculations and is due to the saturation effect in this channel produced by liquid droplets when the water vapor in the atmosphere exceeds ~ 4 g/cm^2 (Prabhakara et. al., 1982). The largest variability is seen in all channels at $\sim$ 42°N which lies in the latitudinal belt of passing baroclinic waves that produce significant changes in precipitation, water vapor and wind.

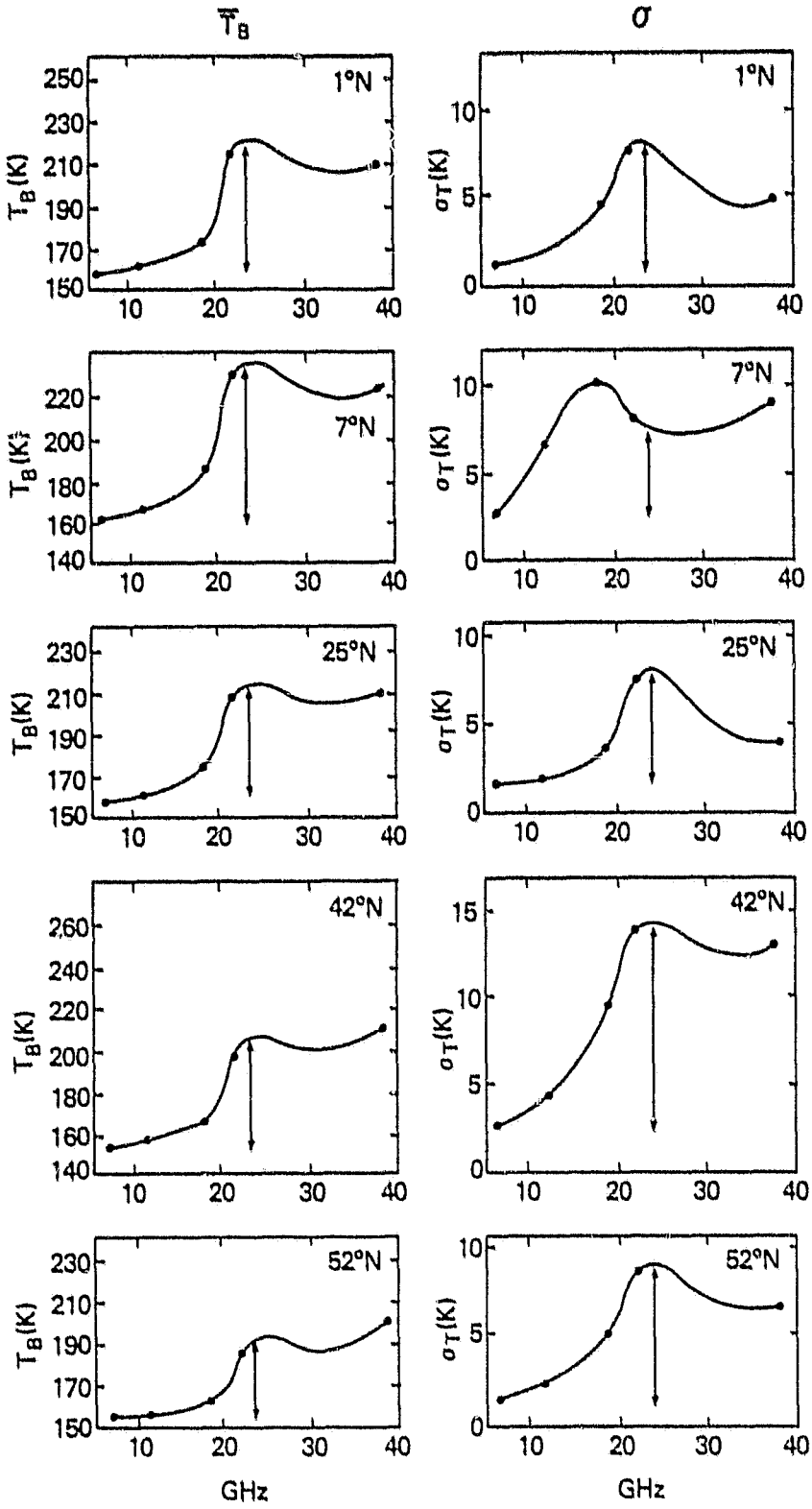

Figure 4. Spectra of zonal mean $\overline{T}_B$ and standard deviation σ of microwave brightness temperature measured by Nimbus 7 SMMR in the vertical polarization. (For an explanation of vertical lines at 22.235 GHz, see text).

The large scale statistical behavior of the data presented above suggests that in the mean the brightness follows the latitudinal distribution of the atmospheric water vapor. The information about the liquid droplets apparently is better revealed by the deviations within the latitudinal zones implying that the spatial and probably the temporal scales of this variable are considerably smaller than that of water vapor.

Another statistical examination of the data consisted of correlations between the various channels on different geographic scales. On large scale, typically going from low latitudes to high latitudes, one finds that there is a significant positive correlation between all channels. Such a correlation amongst the atmospheric channels (18, 21 and 37 GHz) is readily explained in terms of the water vapor and liquid water that increase or decrease the brightness in these channels simultaneously. The positive correlation on large scale between the surface channel at 6.6 GHz and the 21 GHz water vapor channel on the other hand is due to the fact that generally on that scale water vapor in the atmosphere increases or decreases following the sea surface temperature. Contrasting with this positive correlation, on a smaller scale, we find that when samples in localized regions of the subtropical oceans adjacent to the west coasts of continents are considered the correlation between 6.6 GHz and 21 GHz is quite often negative. For example, negative correlation coefficients of 0.2 or more are noticed over the subtropical oceans to the west of north and south American continents. These observations require a physical explanation. In the following sections a meteorological model is developed in order to explain this correlation.

Empirical orthogonal function analysis (see e.g. Holmstrom, 1963; and Smith and Woolf, 1976) of the SMMR data is also performed to assess any further statistical information contained in the microwave measurements. This analysis essentially reinforces the conclusion we arrived at from the simpler statistical examinations presented above.

Sea Surface Temperature Estimation:

The statistical examination of the SMMR data was followed by an empirical examination

in which coincident ship measurements of SST are compared with 6.6 GHz SMMR brightness temperature. These ship observations also contained radiosonde data. Here coincidence is assumed if the satellite data is within 1° latitude and longitude of the ship location and the time difference between the ship and satellite observation does not exceed 1 day. In Figure 5, a set of 30 such comparisons covering a wide range of latitudes, ~ 5°S to ~ 60°N, is shown. The increase in ship SST from about 275 K to 302 K shown along the abscissa crudely reflects the ship latitude in a decreasing order from high latitudes to low latitudes. The day and night satellite measurements are identified in the figure. Taking the ship SST and radiosonde measurements one can estimate theoretically from equation (1) the expected brightness at 6.6 GHz in the absence of surface winds and liquid water in the atmosphere. The solid line shown in Figure 5 neglecting some small scatter in the computed values is derived in this fashion. From this figure we notice the SMMR measurements are widely scattered on one side of the theoretically derived line.

For the sample of ship measurements considered theory predicts a range of ~ 15 K in 6.6 GHz brightness. On the other hand, spread of 6.6 GHz satellite data along the ordinates at 280 K and 300 K amount to about 12 K. This implies that the dynamic range in 6.6 GHz brightness due to SST variation from equator to high latitudes is comparable to the meteorological noise introduced by surface winds and liquid droplets in the atmosphere at some localized regions. Geographically these regions correspond to the mid-latitude and ITCZ rain belts. The night and day observations made by SMMR are identified in Figure 5 to show that the large deviations are not necessarily caused by sun glint.

Despite the meteorological noise problem we notice a significant number of SMMR data lie close to the theoretical line. This empirical analysis of the data suggests that the minimum

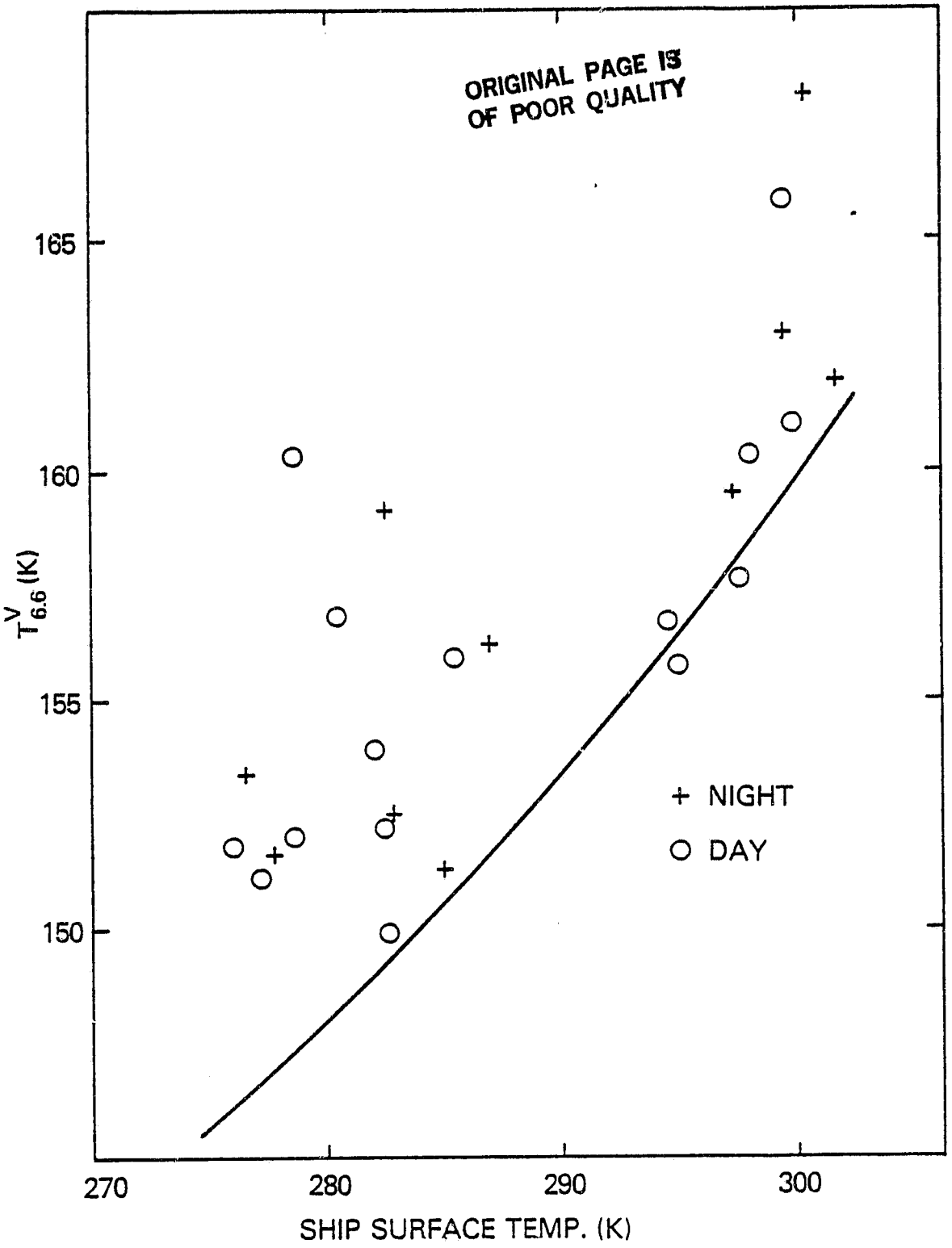

Figure 5. Comparison of brightness temperature at 6.6 GHz (vertical polarization) measured by SMMR and deduced from ship measured sea surface temperature. Solid line represents ship measurements.

in 6.6 GHz brightness temperature observed at a given location over a reasonable length of time probably corresponds to calm surface and fair weather conditions. Based on this reasoning a hypothesis is made, that the minimum measured brightness at 6.6 GHz during a month in a 1° x 1° latitude longitude grid corresponds to a relatively calm surface and fair weather conditions. This hypothesis assumes that the sea surface temperature variability during the course of a month is within the error of our estimation.

Typically during the 30 day period of Oct. 25-Nov. 25, 1978 when the Nimbus 7 SMMR data were acquired every day there are as many as 15 observations in a 1° x 1° grid. While during the period Feb. 15-Mar. 15, 1979 SMMR observations were taken every alternate day and as such there are about half the number of data. For the purpose of estimating a minimum 6.6 GHz brightness from such data it is assumed that there should be at least 5 observations in 1° x 1° grid in the 30 day period. The minimum obtained in this fashion are corrected for water vapor absorption. The water vapor amount in g/cm^2 present in the atmosphere, at the time of the minimum, is deduced from the corresponding 18 and 21 GHz measurements using the scheme given by Prabhakara et al., (1982). This correction amounts to a decrease in 6.6 GHz brightness of 0.3 K per 1 g/cm^2 of water vapor. The corrected $T_{6.6}$ is then converted to T_S using the undisturbed sea surface emissivity (see Fig. 1). As the 6.6 GHz SMMR data have a field of view of ~ 155 Km we have averaged the 1° x 1° grid SST derived above to a grid scale of 2° lat x 3° long. Mean global maps of SST generated in this fashion for the two 30 day periods are shown in Figures 6 and 7. In the process of generating these maps a constant bias of 0.7 K is subtracted from the SMMR 6.6 GHz data for Oct. 25-Nov. 25, 1978 and no correction is made for the second period. This bias is estimated empirically by comparing with ship measurements (National Marine Fisheries Service, NMFS) at high latitudes such as 50° N where the water vapor correction is small.

Excepting for the sidelobe contamination that affects the SMMR 6.6 GHz data to some

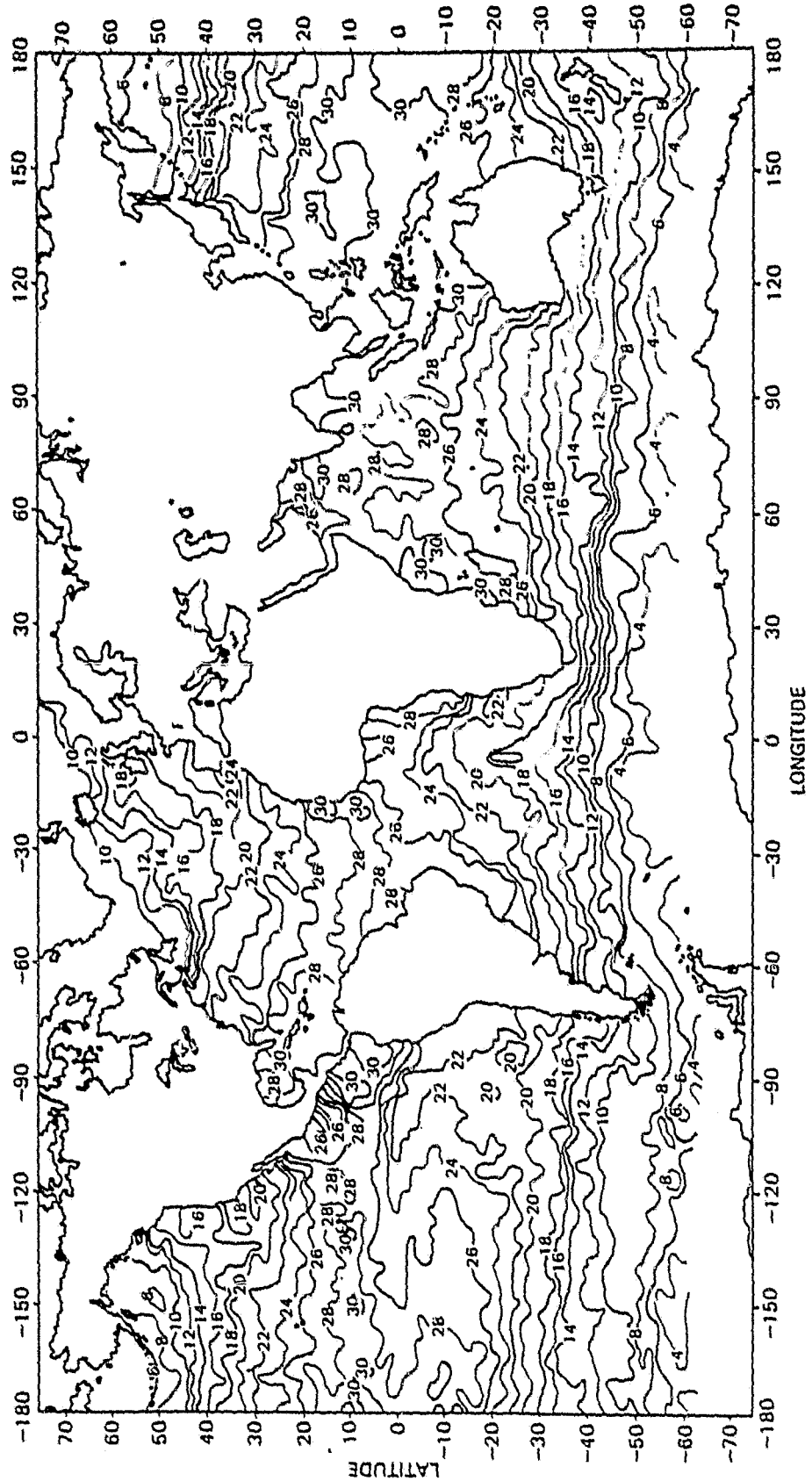

Figure 6. Monthly mean sea surface temperature (°C) derived from Nimbus 7 SMMR for the period Oct. 25-Nov. 25, 1978.

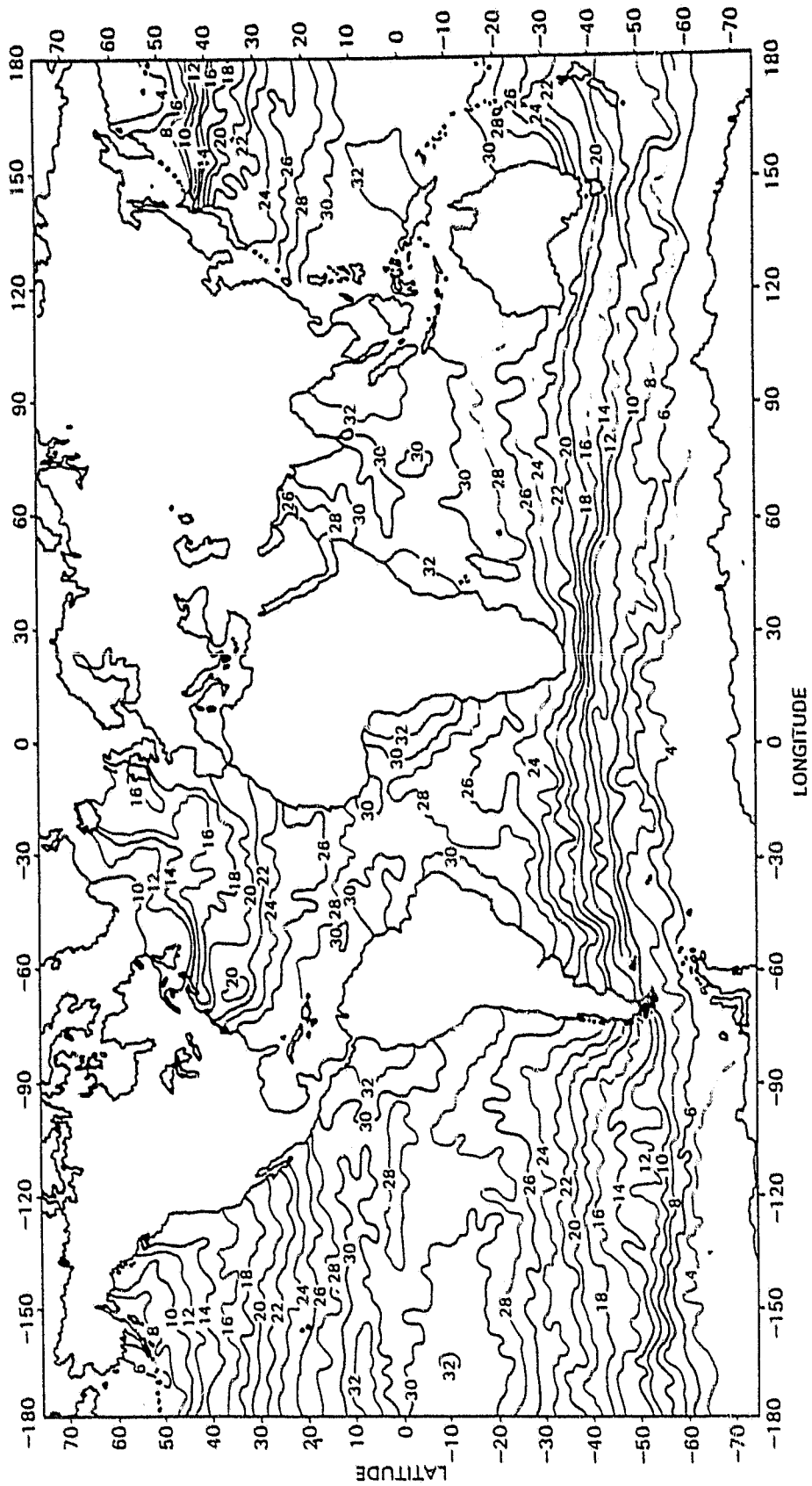

Figure 7. Monthly mean sea surface temperature (°C) derived from Nimbus 7 SMMR for the period Feb. 15-Mar. 15, 1979.

500 km distance from the coasts these SST maps portray the large scale features satisfactorily. The SMMR map of Oct. 25-Nov. 25, 1978 when compared with the NMFS map of SST for Nov. 1978 shows a good agreement over the open ocean. In Figure 8 two comparisons of SST derived from SMMR vs NMFS are shown along the 140°W and 165°W longitudes from 50°.N to 30° S. The comparison shows that the SMMR estimation is within about 1° C of the ship measurements. A significant point to note is that this technique does not suffer from large errors in areas such as ITCZ where there is frequent rainfall. The seasonal change, Nov. 78 to Mar. 79 (See Figures 6 and 7), in SST over the equatorial Pacific and the enhancement in temperature gradient along the circumpolar front in the southern hemisphere shown by SMMR are in good agreement with climatological maps.

One source of systematic error that could not be avoided in the SST analysis is the night and day difference in calibration. This is shown in Figure 9 where the minima in brightness temperature as a function of latitude along 140° W longitude obtained from the night time data and day time data are shown separately. The 6.6 GHz minima during day are smaller than the minima at night in the northern hemisphere while the opposite is true in the southern hemisphere. Obviously when we take a minimum regardless of night or day, as is done in the present SST analysis, these biases are not eliminated. Part of the error in SST estimation from SMMR could be from this source.

Spectral effects produced by liquid droplets and wind:

In the absence of sea ice the microwave brightness temperature T_{B_ν} in 6 to 37 GHz band, over the oceans, can be represented to a good approximation as

$$T_{B_\nu} \cong f(T_S, w, \ell, u) \qquad (7)$$

where T_S in the sea surface temperature, w and ℓ are the total water vapor and liquid water content in the atmosphere, and u is the surface wind speed. The variations introduced in T_{B_ν}

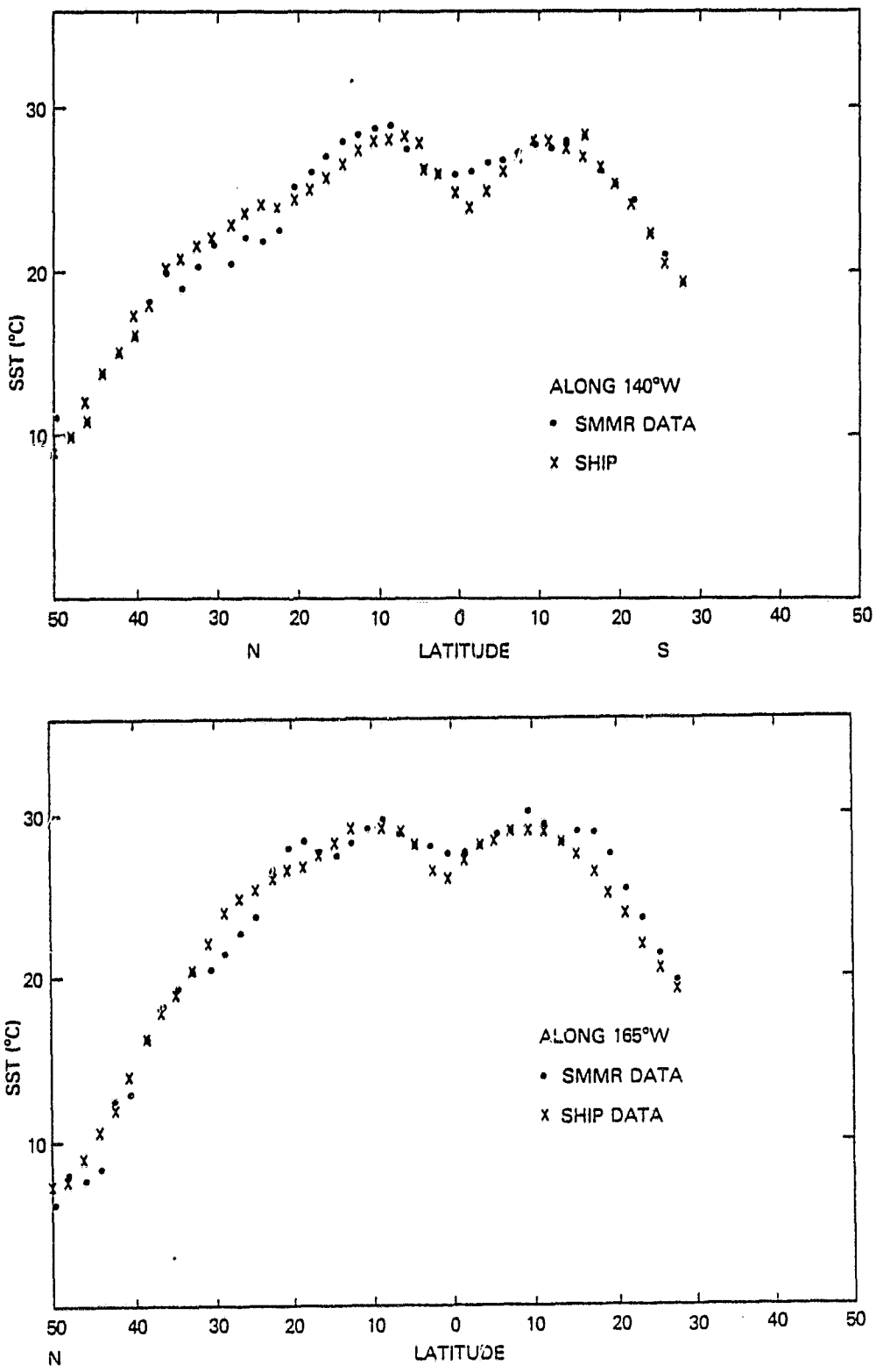

Figure 8. Comparison of sea surface temperature derived from Nimbus 7 SMMR with that obtained from National Marines Fisheries Service for Nov., 1978.

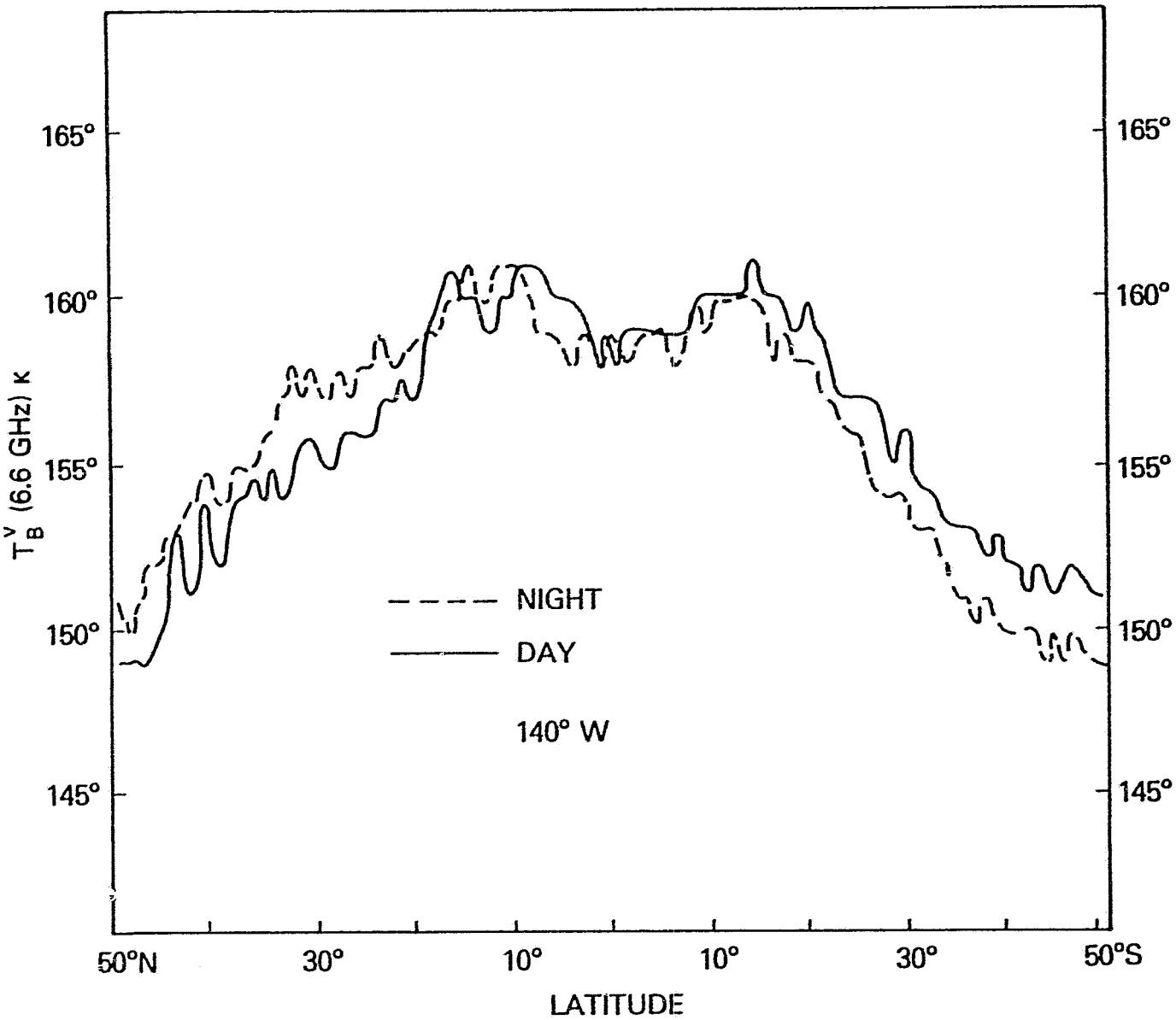

Figure 9. Minima in the Nimbus 7 SMMR 6.6 GHz (vertical polarization) brightness temperature as a function of latitude, along 140° W longitude, obtained from night and day data.

due to the variability in the vertical profiles of the temperature and water vapor in the atmosphere are generally small. Now if we consider cases where the effects of liquid droplets in the atmosphere and surface wind are negligible equation (7) may be written as

$$T^{\circ}_{B_\nu} \cong f^{\circ}(T_S, w^{\circ}) \tag{8}$$

From the discussion presented in the previous section we can consider the SMMR observations in all the channels, at a given location, can be represented by equation (8) when the 6.6 GHz brightness is a minimum during a period of a month at that place. w° is the water vapor content in the atmosphere when $T_{6.6}$ is a minimum. This assumes T_S is close to a constant value in that period and at that location.

Now the deviation δT_{B_ν} in any SMMR channel may be expressed in terms of deviations δw, $\delta \ell$ and δu as follows

$$\delta T_{B_\nu} \cong T_{B_\nu} - T^{\circ}_{B_\nu} \cong \frac{\partial T_{B_\nu}}{\partial w}\,\delta w + \frac{\partial T_{B_\nu}}{\partial \ell}\,\delta \ell + \frac{\partial T_{B_\nu}}{\partial u}\,\delta u \tag{9}$$

This approximation holds good particularly for the surface channels as the non-linearities introduced in the atmospheric channels by the rain are not negligible (Wilheit and Chang, 1980).

These deviations δT_{B_ν}, δw, $\delta \ell$ and δu represent temporal changes at the location under consideration during that month.

Now let us consider the effect of the surface wind. When the wind speed at the sea surface increases the brightness at 6.6 GHz increases due to increase in surface frictional effects. An important effect the surface friction produces is the cross isobaric flow leading to convergence or divergence in the lowest layer of the atmosphere (Philips, 1956; Haltiner, 1971). The strength of such frictionally induced convergence or divergence thus depends on the wind speed. When the flow is divergent the water vapor in the atmosphere over the ocean tends to decrease leading to a decrease in the brightness at 21 GHz water vapor channel. This explains the nega-

tive correlation between the 21 and 6.6 GHz channels observed by SMMR. On the other hand, when there is convergent flow the water vapor increases leading to growth in convection, cloudiness and precipitation. Under these conditions all the SMMR channels show an increase in brightness simultaneously.

With this understanding of the wind induced effects it is desireable to discriminate from the microwave spectral information the divergent and convergent situations. It is found that the surface channels are helpful for this purpose. When we consider the deviations $\delta T_{10.7}$ and $\delta T_{6.6}$ as defined by equation (9) and take their ratio r

$$\text{i.e. } r = \delta T_{10.7}/\delta T_{6.6} \tag{10}$$

we expect the ratio will be close to 1 or smaller when these deviations are produced essentially by changes in the surface conditions induced by divergent flow. However, when there is convergent flow the liquid content together with the water vapor increases in the atmosphere and $\delta T_{10.7} > \delta T_{6.6}$ leading to a significant increase in r value. Theoretical simulations indicate that the value of r is generally greater than 1.2 under such conditions. When this happens the deviations δT_B in the 18, 21, and 37 GHz channels are all positive and quite large compared to $\delta T_{10.7}$. This behavior of data is illustrated in Figure 10A where the latitudinal mean values of δT_B derived from SMMR over the north and south Pacific for the period Oct. 25-Nov. 25, 1978 is shown.

Several interesting details emerge from this figure. All the deviations clearly show large values in the rain belts of the tropics and midlatitudes in the north. Deviations are small in the subtropics, ~ 25°N, and still smaller in the 3°S belt close to the equator. In the southern latitudes these tropical, subtropical, and midlatitude belts are not as clearly defined. The deviations $\delta T_{10.7}$ in almost all latitudes are about twice as large as that at 6.6 GHz. Based on the sensitivities (See Table 1) in these channels this can be accounted for mainly in terms of

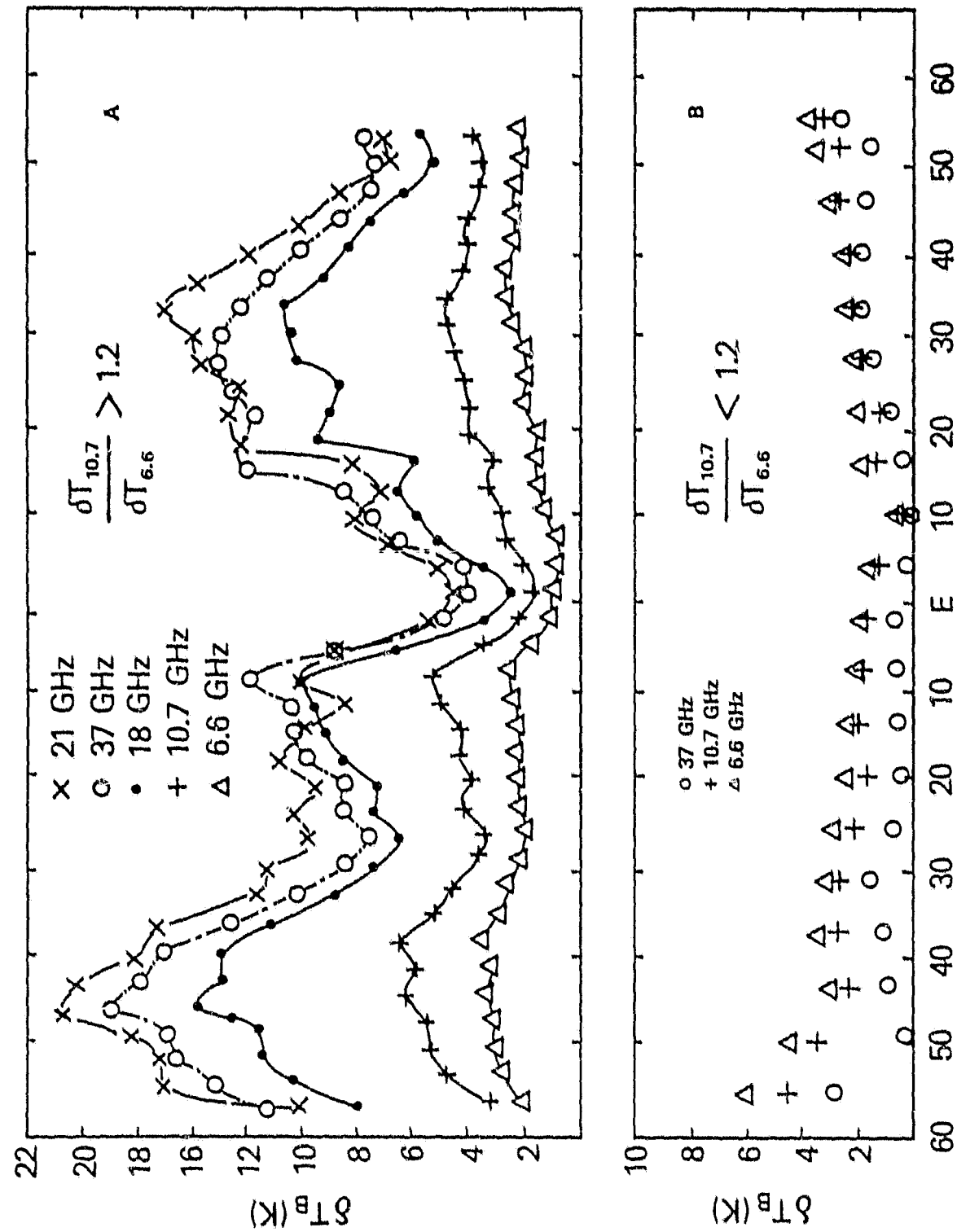

Figure 10. Zonal mean of deviations in the Nimbus 7 SMMR brightness temperatures for convergent flow (A); and for divergent flow (B).

the liquid drops and very little due to water vapor changes. The deviations at 18, 21 and 37 GHz in the tropical rain belt are smaller than those in the midlatitudes.

A combination of several processes are needed to explain these observations. Temporal changes in water vapor in the tropical rainbelts is small compared to that in the midlatitude baroclinically active rainbelts. Based on an earlier study (Prabhakara et al., 1982) it is possible to estimate the deviations in the water vapor given the deviations at 18 and 21 GHz.

Close to 40°N (See Figure 10A) latitude we can infer on the average about 1 g/cm^2 increase in water vapor when significant amount of liquid water droplets are present. In the tropics such an inferred increase is only about 0.3 g/cm^2. The second and probably a more serious consideration is the effect of rain. For rain droplets Rayleigh approximation breaks down as the frequency increases. As a consequence in the presence of rain SMMR brightness measurements at high frequencies 18, 21 and 37 GHz do not increase linearly with the liquid water content in the atmosphere. This non-linear response progressively inhibits growth in brightness as the frequency increases (Wilheit and Chang, 1980). Furthermore, the rain cells are likely to be more intense and smaller in size in the convectively active tropics as compared to that in the baroclinically active midlatitudes. The combined effect of non-linear response and cell size could explain in good part the smaller deviation at 18, 21 and 37 GHz in the tropical rain belts as compared to those in the midlatitudes.

A similar analysis of the microwave data in which $\delta T_{10.7}/\delta T_{6.6} < 1.2$ is shown in Figure 10B. The influence of tropical and midlatitude rainbelts is practically absent in these data. The 18, 21, and 37 GHz channels show somewhat smaller deviations than the surface channels. These microwave data represent divergent flow conditions in the lowest layers of the atmosphere.

The discussion of the SMMR data presented so far can be summarized in the form of a meteorological model as shown in Figure 11. The brightness temperature spectrum between

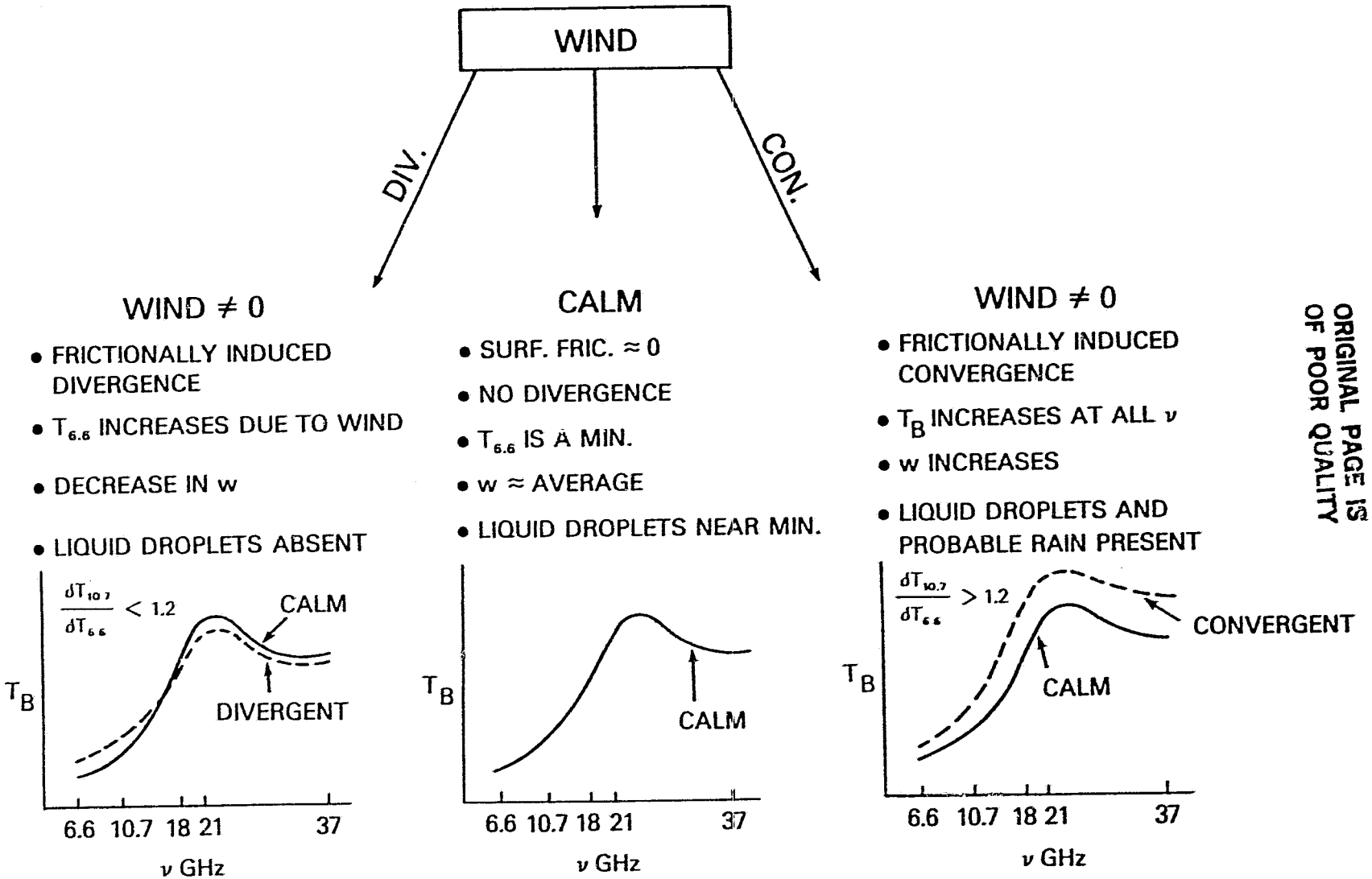

Figure 11. Meteorological model relating the Nimbus 7 SMMR microwave brightness temperature spectral characteristics to the divergent, convergent and non-divergent wind fields.

6.6 to 37 GHz corresponding to calm surface conditions, when minimum in 6.6 GHz brightness is observed, is shown by a solid line in the inset figures. The modified spectra produced by divergent and convergent flow are shown by dashed curves.

The reasons for choosing the minimum brightness at 6.6 GHz to determine the sea surface temperature is more vividly brought out by the meteorological model. From this model we note the liquid information may be derived from the convergent situations, while the surface wind information is best revealed when the surface flow of air is divergent.

Estimation of liquid water content:

From the analysis presented in the previous sections we note the information contained in the 18, 21 and 37 GHz atmospheric channels is very sensitive to liquid water in the clouds, rain droplets and water vapor. The non-linear effects introduced by rain droplets, in these channels increase considerably with frequency. As the interest in this study is limited to estimation of liquid water in the atmosphere we have restricted our attention to the lower frequencies of 6.6 and 10.7 GHz where the Rayleigh approximation is satisfactory for both the liquid droplets in the clouds and rain.

When convergent conditions exist the difference between the deviations at 10.7 and 6.6 GHz may be used to deduce the liquid water content in the atmosphere as follows

$$\ell = a(T) \, [\delta T_{10.7} - \delta T_{6.6}] \qquad (11)$$

where the deviations $\delta T_{10.7}$ and $\delta T_{6.6}$ are obtained according to the definition given by equation (9) and a(T) is a coefficient that depends on the temperature of the liquid drops. The absorption due to the droplets decreases as the temperature increases by about a factor of 3 going from - 20°C to + 20°C. Taking the temperature dependence into account theoretical calculations are made to determine the liquid droplet effect. In these calculations

several radiosonde profiles on the oceans ranging from warm and humid low latitudes to cold and dry high latitudes are considered. For each one of these model atmospheres $T_{10.7}$ and $T_{6.6}$ are calculated with no liquid water in the atmosphere. Then the two brightnesses are again calculated adding to each model atmosphere a 1 km thick liquid droplet cloud with its base 1 km above the sea surface. The difference in brightness $\delta T_{10.7}$ and $\delta T_{6.6}$ due to the liquid in the clouds is deduced for each case. In Figure 12 we present the effect of such a cloud containing 50 mg/cm^2 of liquid droplets as a function of sea surface temperature. The difference $\delta T_{10.7} - \delta T_{6.6}$ for the same liquid content in the clouds increases as the SST decreases. This is mainly because the temperature of the atmosphere, in which the cloud is imbedded, decreases in a gross sense following the SST.

The liquid water content in the atmosphere is estimated from SMMR measurements with the help of this theoretical model. SMMR data that satisfy the condition $\delta T_{10.7} / \delta T_{6.6} > 1.2$ are used for liquid water estimation. Such data constitute about 30% of all the observations. Since we know the monthly mean SST from SMMR, for a given $(\delta T_{10.7} - \delta T_{6.6})$ the liquid water can be estimated from Figure 12. Actually the following equation (12) that fits the curve in Figure 12 is used in the liquid water estimation

$$\ell = 20 \times (\delta T_{10.7} - \delta T_{6.6}) \Big/ \text{Exp}\left(\frac{31 - T_S}{35}\right) \qquad (12)$$

when $r > 1.2$

Here T_S is in °C, and ℓ is expressed in mg/cm^2.

Global maps of average liquid water in the atmosphere for the two 30 day periods are derived in this fashion. These maps are shown in Figures 13 and 14.

A relevant detail in obtaining the deviations $\delta T_{10.7}$ and $\delta T_{6.6}$ should be mentioned at this point. The minima in the 6.6 and the corresponding 10.7 brightnesses in each 30 day period were determined separately for night and day at each grid box of 1° x 1° size. Then

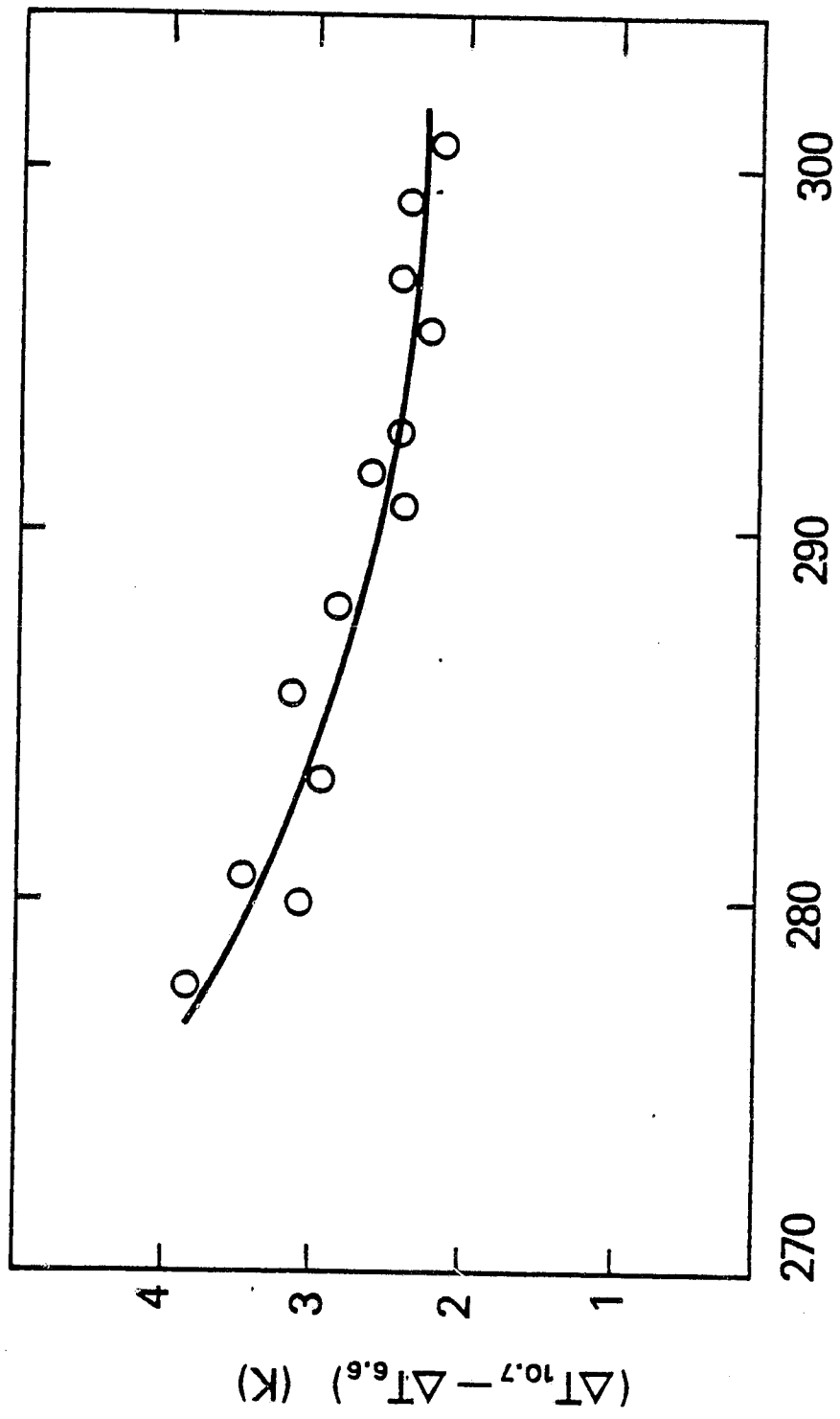

Figure 12. Dependence of liquid droplet (cloud or rain) absorption, $\Delta T_{10.7} - \Delta T_{6.6}$, on temperature. Liquid droplet content = 50 mg/cm^2.

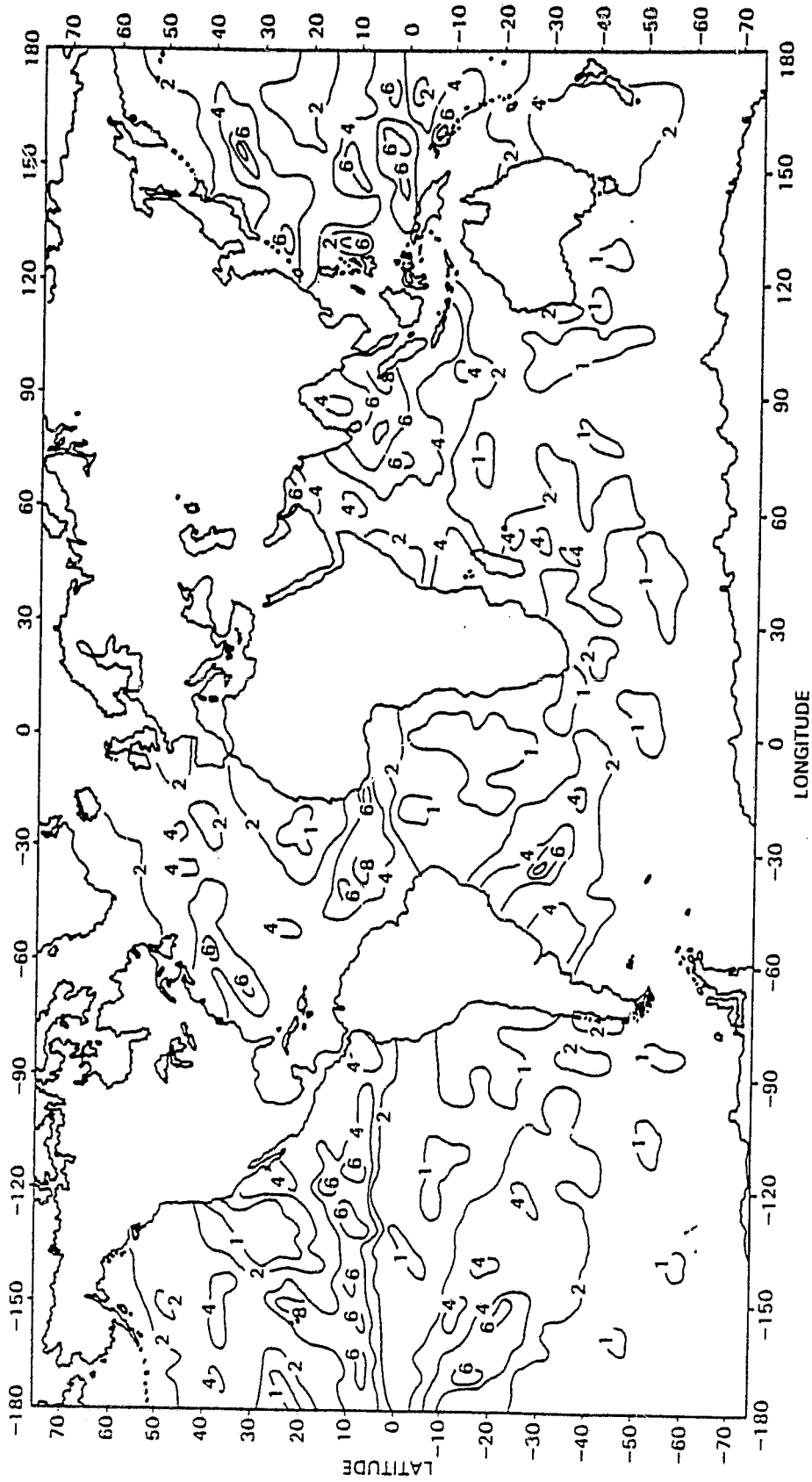

Figure 13. Liquid water content (10^{-2} g/cm^2) in the atmosphere deduced from Nimbus 7 SMMR for the period Oct. 25-Nov. 25, 1978.

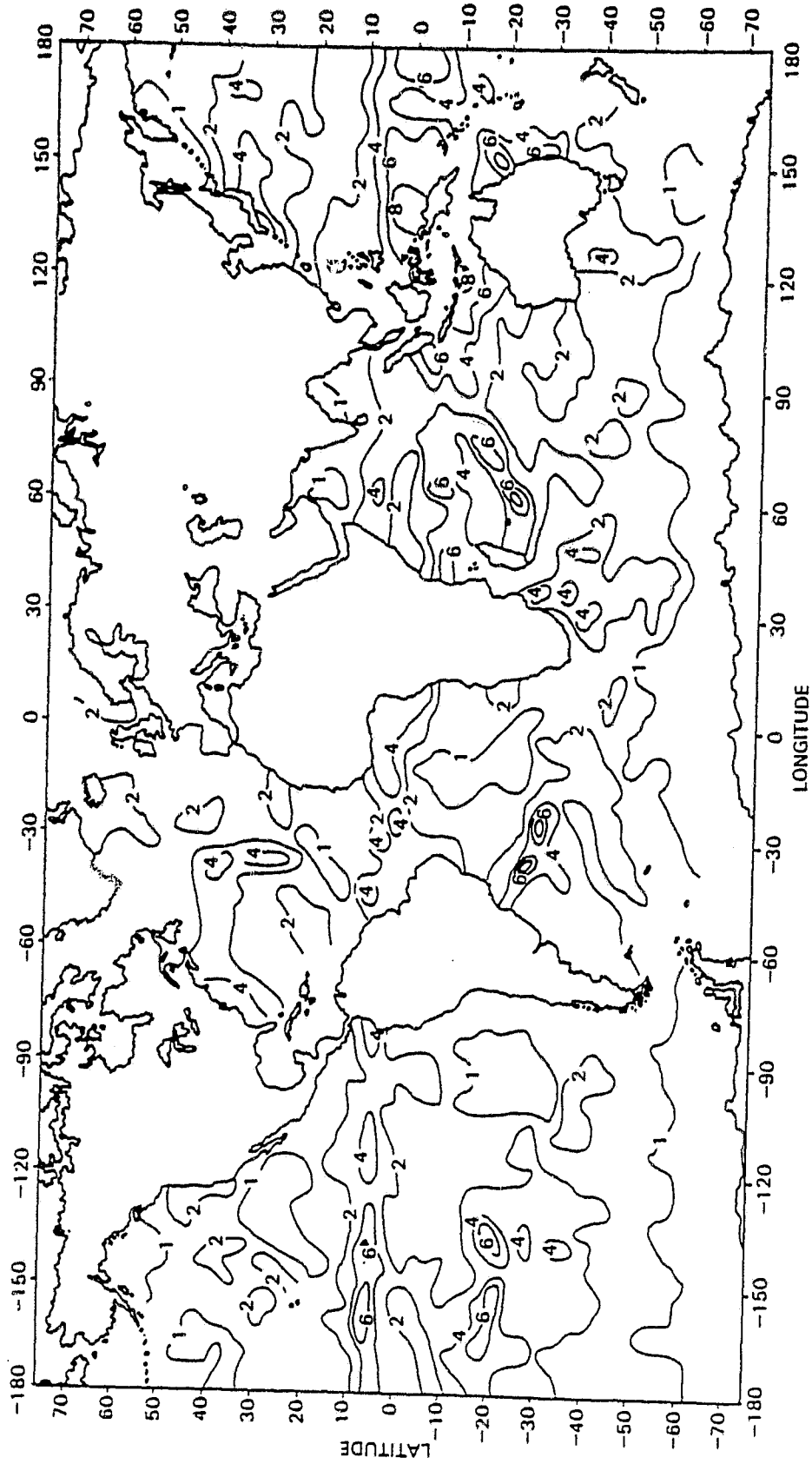

Figure 14. Liquid water content (10^{-2} g/cm^2) in the atmosphere deduced from Nimbus 7 SMMR for the period Feb. 15-Mar. 15, 1979.

deviations for each SMMR channel were obtained separately for day and night and then averaged. By following this procedure the systematic calibration errors between night and day could be alleviated. The relatively weak water vapor absorption effect in these 6.6 and 10.7 GHz channels is neglected.

Several interesting details in the 30 day mean liquid water maps may be noted. The ITCZ is clearly manifested in the northern hemisphere with large liquid water content sometimes approaching 80 mg/cm^2. The position of this ITCZ apparently moves from about 7°N to 5°N from Oct-Nov to Feb-Mar. The regions of warm ocean currents in the north and south hemispheres are associated with significant liquid water in the atmosphere. All the subtropical subsidence regions to the west of the continents are distinguishable by the minima in liquid water content reaching values as small as 10 mg/cm^2.

These maps of liquid water cannot be readily compared with maps generated from conventional data. In a study made by Grody et al., (1980) a map of the liquid water in the atmosphere over the Pacific Ocean between 35°N to 35°S was derived for the period Aug. 18-Sept. 4 1975 using the Scanning Microwave Spectrometer data (SCAMS) from Nimbus 6. Some salient features of the liquid water distribution shown in our maps are also revealed in the map of Grody et al. However, it appears that the technique used here has a better sensitivity enabling us to sense values as small as 10 mg/cm^2 of liquid water. This sensitivity has enabled us to extend our analysis to 50°N and 50°S.

Since there is no ground truth to compare with we cannot establish an accuracy to our liquid water estimation. But conservatively, from theoretical considerations. we assess the accuracy should be ~ 10 mg/cm^2.

Estimation of Surface Wind Speed:

The Nimbus 7 SMMR data that do not reveal liquid droplet effect, i.e. $\delta T_{10.7}/\delta T_{6.6} < 1\text{-}2$ constitute about 70% of the total observations. These observations are analyzed for the wind information.

The 10.7 GHz measurements are more sensitive to surface wind than the measurements at 6.6 GHz (Wilheit, 1979). For this reason the wind information is deduced from 10.7 GHz data. The monthly mean deviations $\delta T_{10.7}$ are estimated taking into account properly the night and day calibration errors that were pointed out earlier. The mean deviation maps derived in this manner for the two 30 day periods are shown in Figures 15 and 16.

These deviations in the 10.7 GHz are attributed to the surface winds. In order to interpret these deviations in terms of wind speed we have adopted with minor modifications the empirical model of the surface emissivity change vs wind speed developed by Wentz (1981) based on simultaneous measurements made by the Seasat Scatterometer and SMMR. Accordingly at 10.7 GHz vertical polarization the change $\Delta\epsilon$ in the surface emissivity under conditions of neutral stability is given by

$$\begin{aligned} u &= \Delta\epsilon_{10.7} \times 1.4 \times 10^3 \quad \text{when } u < 13 \text{ m/s} \\ u &= 13 + (\Delta\epsilon_{10.7} - D.01) \times 4.2 \times 10^3 \quad \text{when } u > 13 \text{ m/s} \end{aligned} \tag{13}$$

where $\Delta\epsilon_{10.7} = \delta T_{10.7}/T_S$ and u is wind speed at 20 m height above sea surface.

Following this model surface wind speed is deduced from SMMR data as shown in Figures 17 and 18.

In order to compare these sea surface winds, the ship measured winds are averaged in a

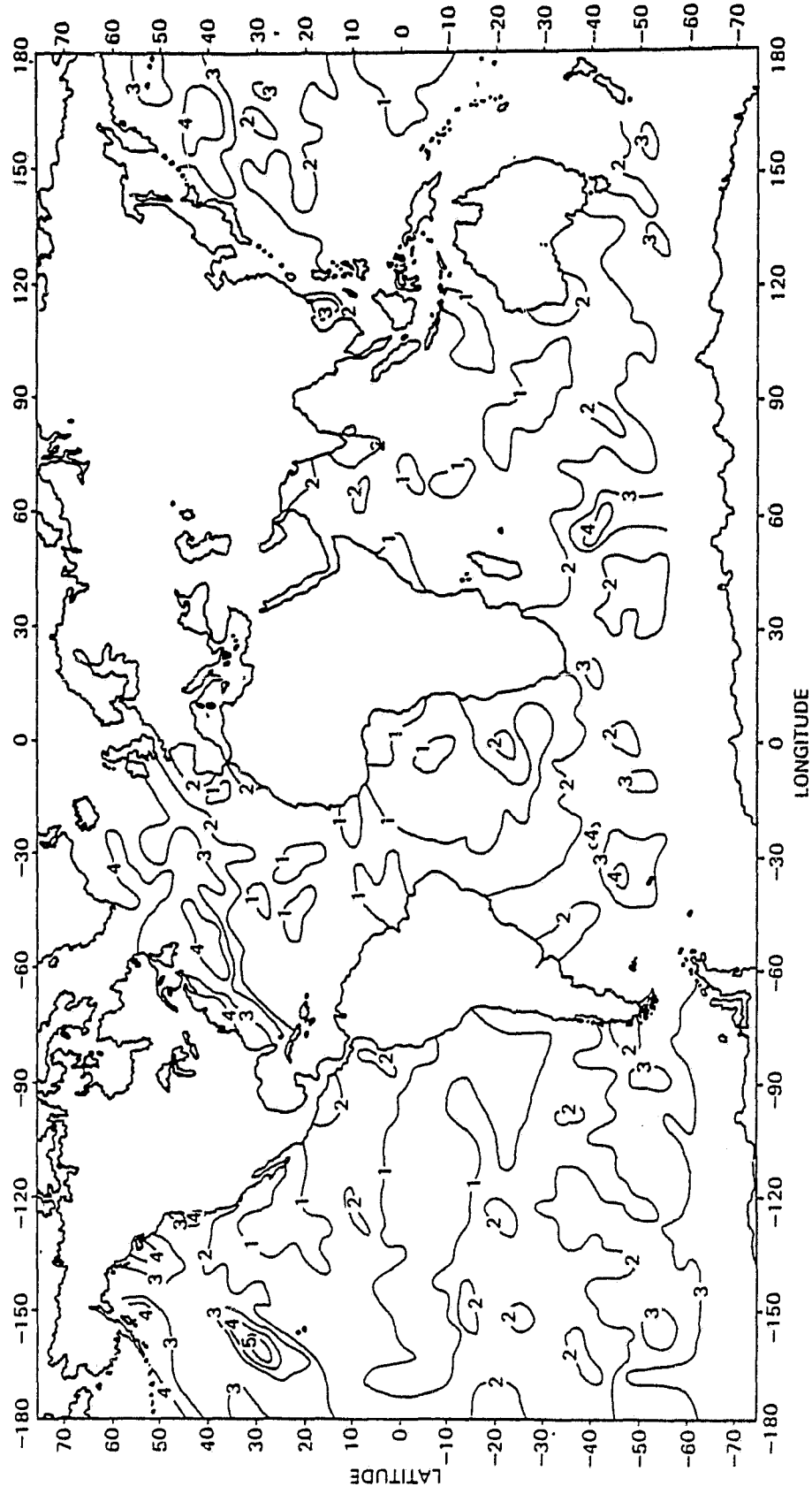

Figure 15. Brightness temperature change $\delta T^{V}_{10.7}$ (K) due to wind during 25 Oct.- 25, Nov., 1978.

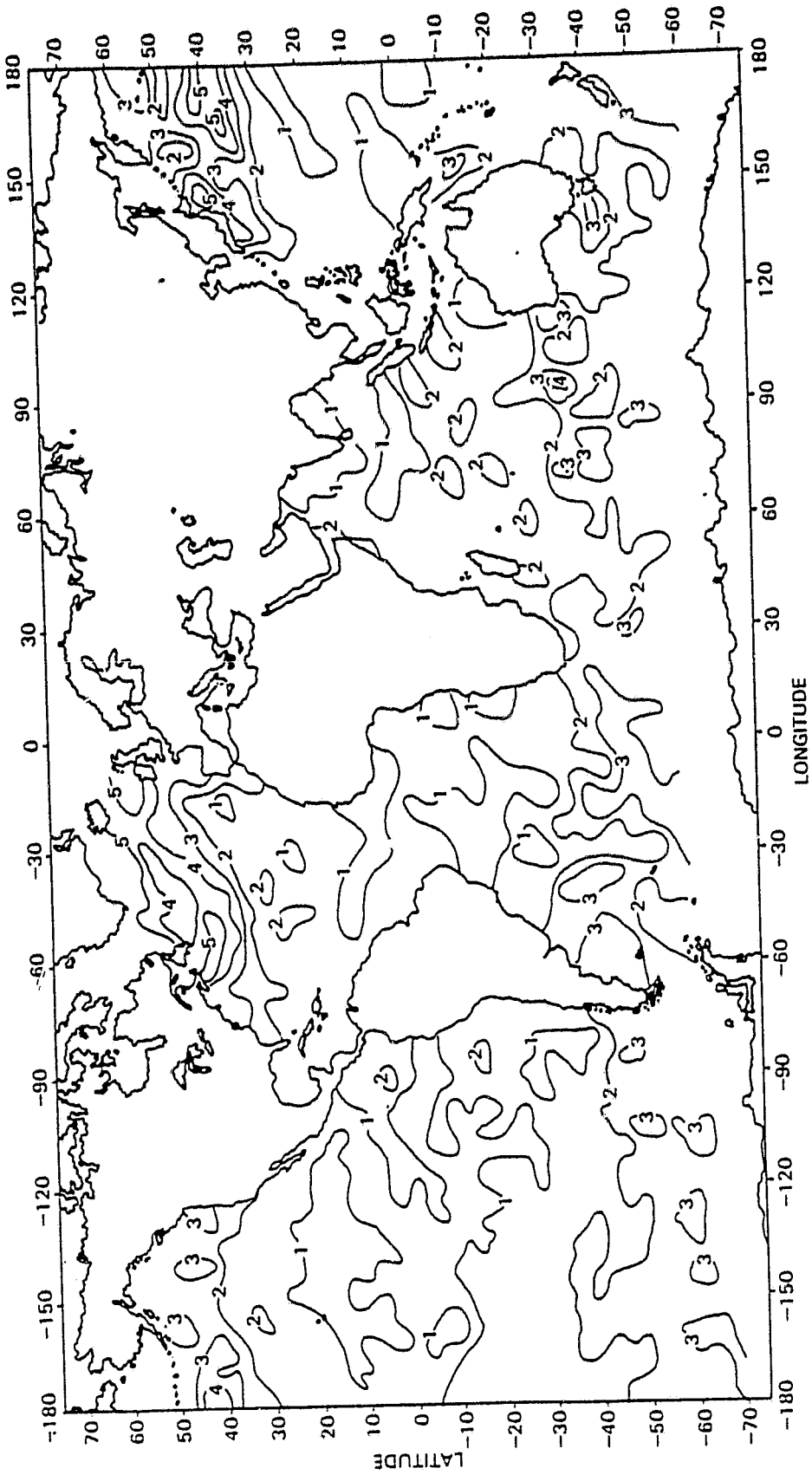

Figure 16. Brightness temperature change $\delta T^{V}_{10.7}$ (K) due to wind during 15 Feb-15 Mar., 1979.

ORIGINAL PAGE IS
OF POOR QUALITY

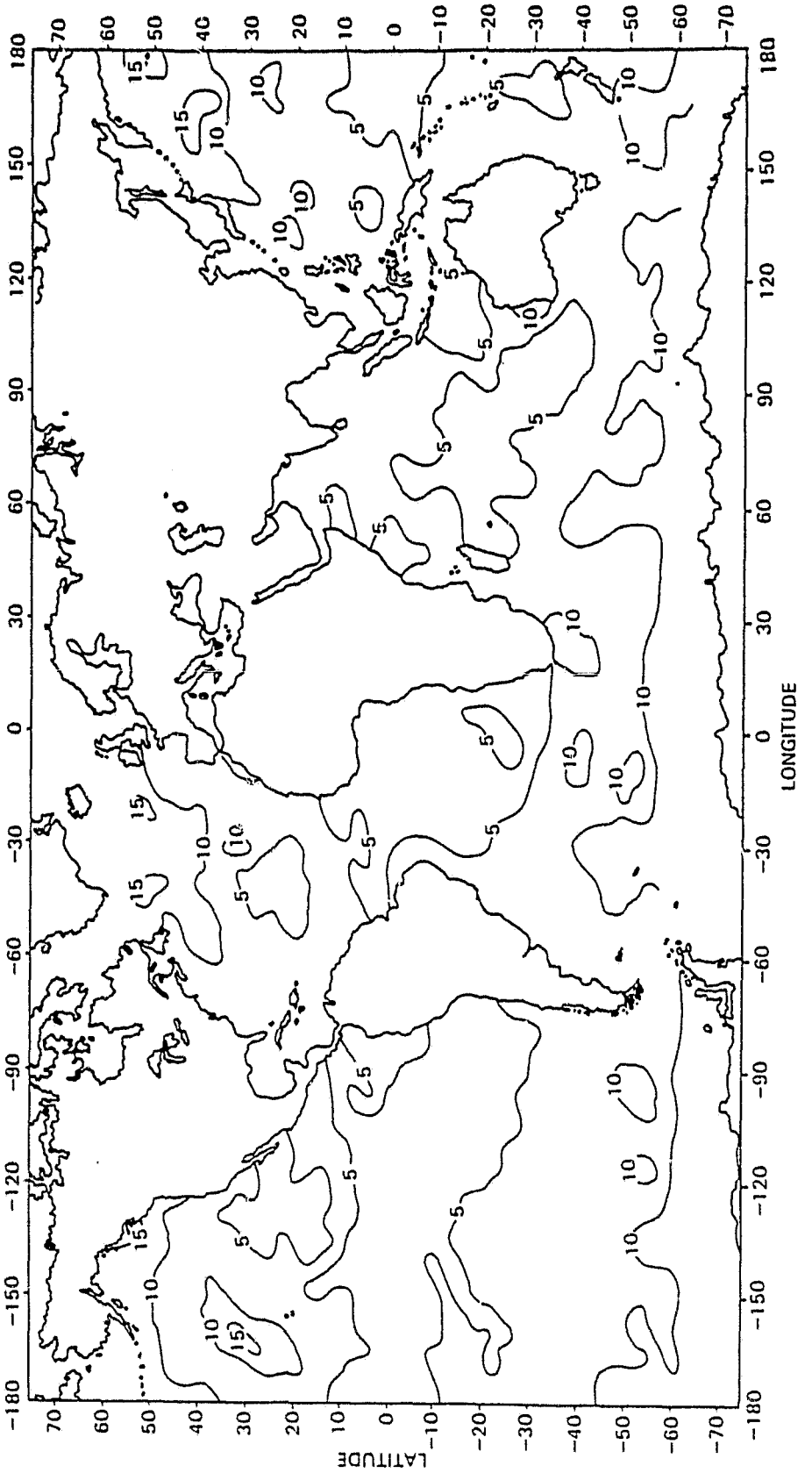

Figure 17. Wind speed (m/s) derived from Nimbus 7 SMMR for the period 25 Oct.-25 Nov., 1978.

ORIGINAL PAGE IS
OF POOR QUALITY

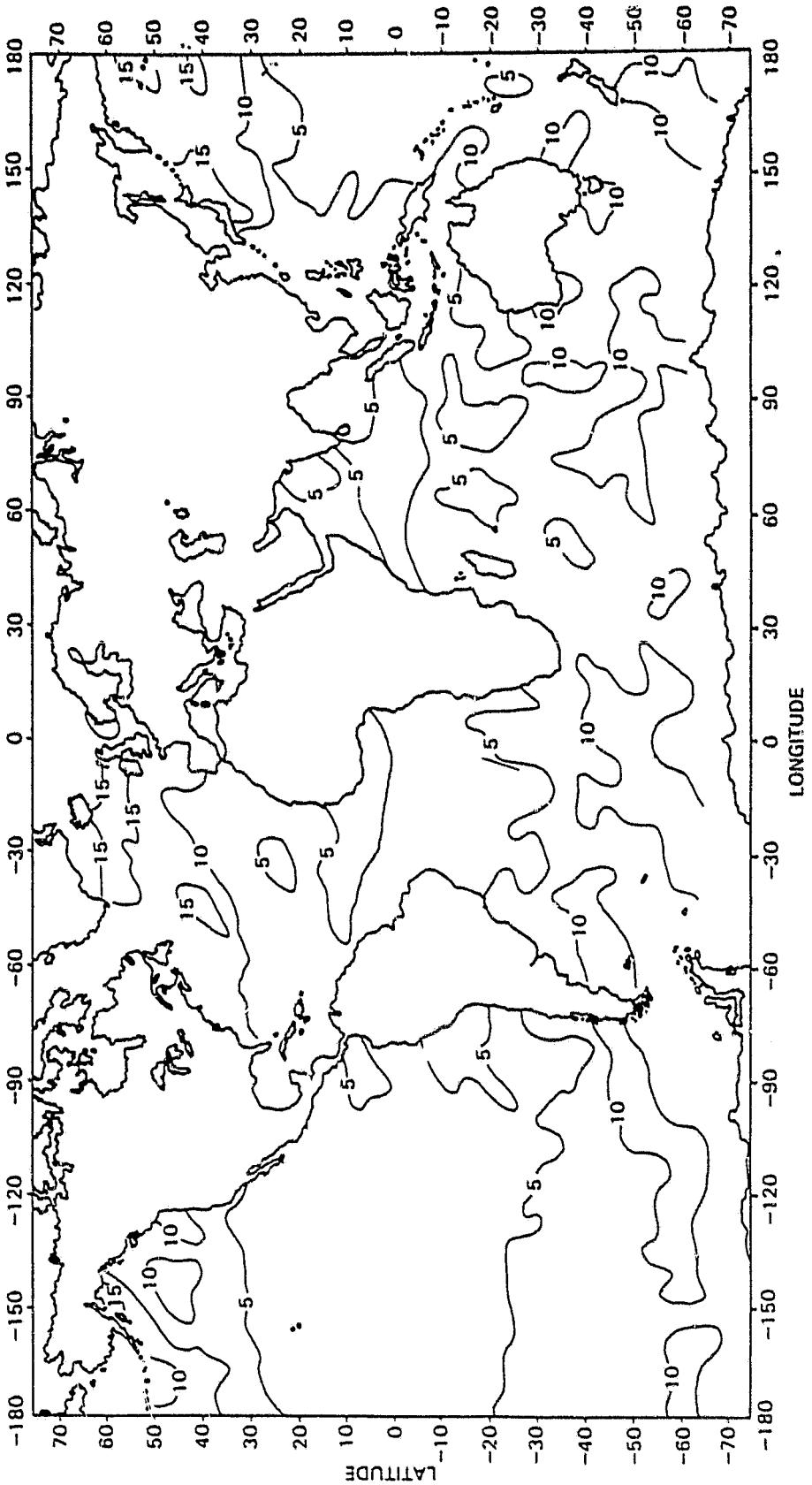

Figure 18. Wind speed (m/s) derived from Nimbus 7 SMMR for the period 15 Feb.-15 Mar., 1979.

similar manner and are presented in Figures 19 and 20. The ship measurements are plentiful over the North Atlantic and North Pacific. However, observations in several other areas tend to be sparse. In order to indicate this lack of information in Figures 19 and 20 the isolines derived from 5 or fewer days of observations are dashed. The satellite sensed surface winds and that of the ships reveal several common features and fair agreement, particularly over the North Atlantic where the ship data are abundant. The large wind speeds 10 to 15 m/s observed over the warm ocean current regions such as the gulf stream and Kuroshio, and weak winds < 5 m/s over some subtropical and tropical regions revealed by SMMR are shown by ship observations also. In view of the fact that the ship and satellite data are not sampled similarly in time and in space, and furthermore no stability corrections (Cardone, 1969) were applied to satellite wind estimates we can not compare the two sets of measurements more thoroughly. However a rough estimate of the wind speed accuracy given by this technique is ~ 2.5 m/s.

The determination of wind speed in the presence of significant amount of liquid droplets in the atmosphere has not been satisfactory. There is a good probability that the wind speed is correlated with the liquid droplet content in the atmosphere when convergent flow is present. As the brightness change at 10.7 GHz due to liquid droplets is substantial the wind induced brightness variation could not be satisfactorily separated.

Summary and Conclusions:

The Nimbus-7 SMMR observations demonstrate that the 6.6 GHz brightness temperature is increased minimally by liquid droplets, in clouds and rain, and by water vapor in the atmosphere. This property is very helpful to estimate the sea surface temperature from satellite observations. However, the surface winds also increase the microwave brightness. For this reason a minimum observed brightness in the 6.6 GHz, at a given region over a period of few weeks, is selected to estimate the sea surface temperature. This procedure assumes that the minimum

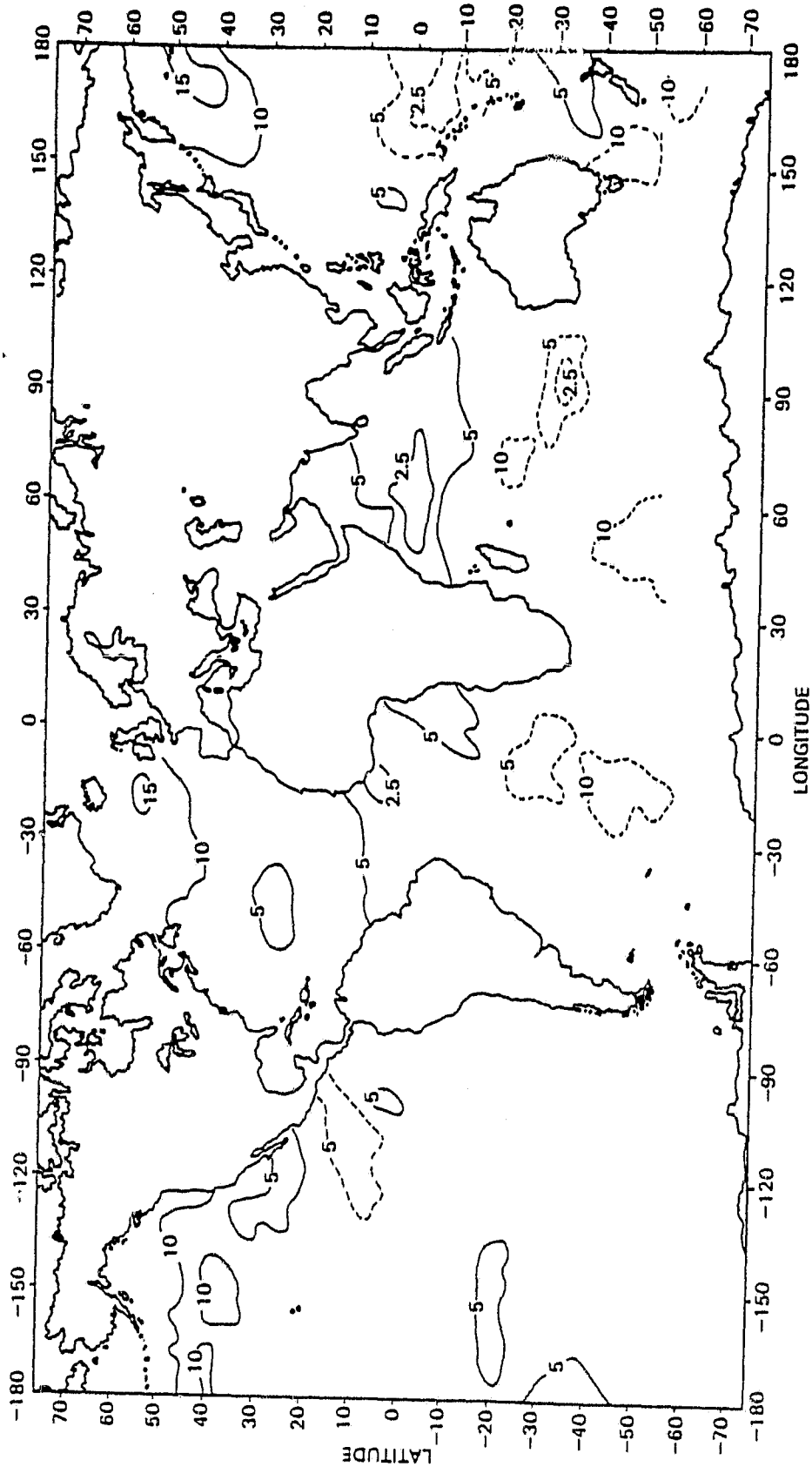

Figure 19. Ship measured wind speed (m/s) for the month of Nov., 1978.

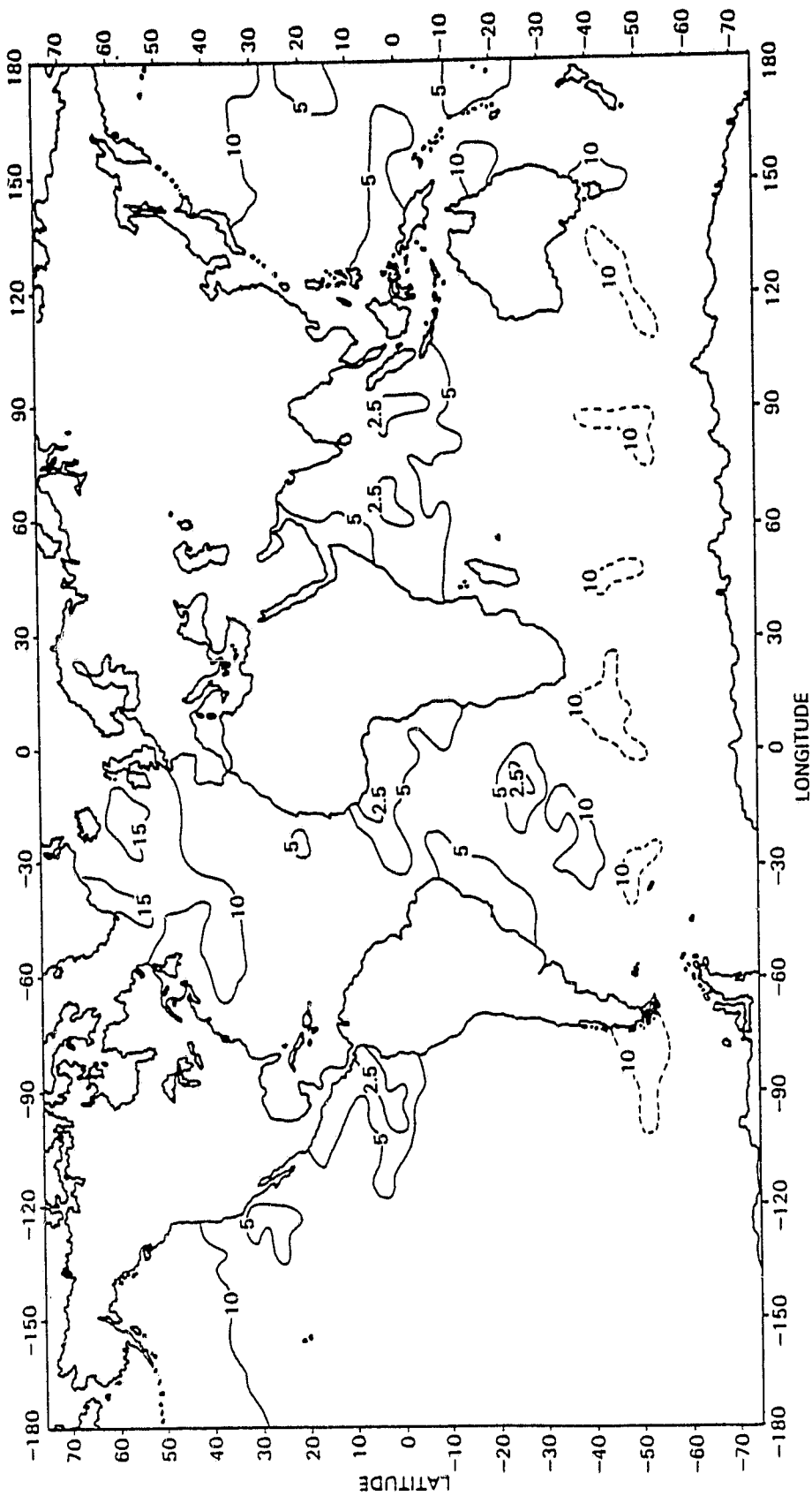

Figure 20. Ship measured wind speed (m/s) for 15 Feb–15 Mar., 1979.

in brightness coresponds to neglible wind speed at the surface and a small amount of liquid droplets in the atmosphere, and further the variability in the sea surface temperature is within the accuracy of our estimation. Once a minimum in the 6.6 GHz brightness at a given location is identified the estimation of surface wind speed and liquid droplet content in the atmosphere can be done from temporal changes in the 6.6 and 10.7 GHz channels. These ideas which are crucial to the remote sensing technique developed in this study are tested with a large body of Nimbus-7 SMMR data over the global oceans. The satisfactory information obtained on the sea surface temperature, surface wind speed and liquid water content in the atmosphere supports these basic view points.

For the estimation of liquid water content in the atmosphere, either in the form of clouds or rain, the measurements at long wavelengths, 6.6 and 10.7 GHz, are useful. This is mainly because at these wavelengths the water vapor absorption is very weak and non-linear effects introduced by rain droplets are not significant.

The empirical model of the sea surface emissivity vs surface wind speed developed by Wentz (1981) with the help of Seasat Scatterometer and SMMR seems to take into account in a gross fashion the effects of sea surface roughness and foam.

The sea surface temperature can be measured by both the infrarred and microwave techniques. The infrared technique can yield small spatial resolution measurements in cloud free areas (see for e.g. McClain et al., 1982). On the other hand microwave measurements permit SST estimation over a large field of view in the presence of non-raining light clouds when the meteorological conditions at the surface are reasonably calm. The sea surface temperature maps derived from Nimbus 4 Infrared Interferometer data (Prabhakara et al., 1979), which have a field of view of about 100 km. may be compared with the SMMR sea surfaces temperature maps. From such a comparison we conclude that for 100 to 200 km spatial resolution the microwave measurements, away from coastal areas, can yield better sea surface temperature

information mainly because of the ability to probe through light clouds. From the above discussion we find the infrared and microwave sea surface temperature sensing abilities are complimentary to one another. The two techniques together can satisfy the needs of scientific studies that require sea surface temperature measurements on different spatial and temporal scales.

The Nimbus 7 SMMR has produced several years of useful observations. The information on the sea surface temperature, surface wind speed, liquid water and water vapor content in the atmosphere that can be derived on the global oceans, from this long record of SMMR data, will be valuable to climate studies.

ACKNOWLEDGEMENTS:

We are grateful to Dr. T. T. Wilheit for his encouragement and constructive criticism. The help given by Mr. Hyo D. Chang in the initial phases of this work is appreciated. We are thankful to Dr. T. H. Lee for programming support.

FIGURE CAPTIONS

Figure 1. Variations of smooth sea surface emissivity as a function of temperature for SMMR frequencies at incidence angle of 50°.

Figure 2. Microwave absorption coefficient for liquid water droplets as a function of frequency and temperature.

Figure 3. Microwave absorption coefficient for atmospheric water vapor as a function of frequency at sea level pressure.

Figure 4. Spectra of zonal mean $\bar{T}$ and standard deviation σ of microwave brightness temperature measured by Nimbus 7 SMMR in the vertical polarization. (For an explanation of vertical lines at 22.235 GHz, see text).

Figure 5. Comparison of brightness temperature at 6.6 GHZ (vertical polarization) measured by SMMR and deduced from ship measured sea surface temperature. Solid line represents ship measurements.

Figure 6. Monthly mean sea surface temperature (°C) derived from Nimbus 7 SMMR for the period Oct. 25-Nov. 25, 1978.

Figure 7. Monthly mean sea surface temperature (°C) derived from Nimbus 7 SMMR for the period Feb. 15-Mar. 15, 1979.

Figure 8. Comparison of sea surface temperature derived from Nimbus 7 SMMR with that obtained from National Marines Fisheries Service for Nov., 1978.

Figure 9. Minima in the Nimbus 7 SMMR 6.6 GHz (vertical polarization) brightness temperature as a function of latitude, along 140°W longitude, obtained from night and day data.

Figure 10. Zonal mean of deviations in the Nimbus 7 SMMR brightness temperatures for convergent flow (A); and for divergent flow (B).

Figure 11. Meteorological model relating the Nimbus 7 SMMR microwave brightness temperature spectral characteristics to the divergent, convergent and non-divergent wind fields.

Figure 12. Dependence of liquid droplet (cloud or rain) absorption, $\Delta T_{10.7} - \Delta T_{6.6}$, on temperature. Liquid droplet content = 50 mg/cm^2.

Figure 13. Liquid water content (10^{-2} g/cm^2) in the atmosphere deduced from Nimbus 7 SMMR for the period Oct. 25-Nov. 25, 1978.

Figure 14. Liquid water content (10^{-2} g/cm^2) in the atmosphere deduced from Nimbus 7 SMMR for the period Feb. 15-Mar. 15, 1979.

Figure 15. Brightness temperature change $\delta T^V_{10.7}$ (K) due to wind during 25 Oct.-25 Nov., 1978.

Figure 16. Brightness temperature change $\delta T^V_{10.7}$ (K) due to wind during 15 Feb.-15 Mar., 1979.

Figure 17. Wind speed (m/s) derived from Nimbus 7 SMMR for the period 25 Oct.-25 Nov., 1978.

Figure 18. Wind speed (m/s) derived from Nimbus 7 SMMR for the period 15 Feb.-15 Mar., 1979.

Figure 19. Ship measured wind speed (m/s) for the month of Nov., 1978.

Figure 20. Ship measured wind speed (m/s) for 15 Feb.-15 Mar.. 1979.

REFERENCES

Cardone, V. J., 1969. 'Specification of wind distribution in the marine boundary layer for wave forecasting' Ph.D. dissertation, New York Univ., Dept. of Meteorol. and Oceanography (Available from NTIS order no. AD702690).

Chang, A. T. C. and T. T. Wilheit, 1979. 'Remote sensing of atmospheric water vapor, liquid water, and wind speed at the ocean surface by passive microwave techniques from Nimbus 5 satellite' Radio Science, Vol. 14, pp 793-803.

Cox, C. and W. Munk, 1955. 'Some problems in optical oceanography' Jour. of Marine Res., Vol. 4, pp 63-78.

Gloersen, P., and L. Hardis, 1978. 'Scanning multichannel microwave radiometer (SMMR) experiment' Nimbus 7 Users' guide, C. R. Madrid, Ed., NASA/Goddard Space Flight Center, Greenbelt, Maryland, pp 213-245.

Gloersen, P., and F. T. Barath, 1977. 'A scanning multichannel microwave radiometer for Nimbus-G and Seasat-A' IEEE J. Oceanic Eng., Vol OE. 2, No. 2.

Grody, N. C., A. Gruber and W. C. Shen, 1980. 'Atmospheric water vapor content over the tropical Pacific derived from Nimbus-6 Scanning Microwave Spectrometer'. Jour. Appl. Meteor., Vol. 19, pp 986-996.

Gunn, L. L. S. and T. W. R. East, 1954. 'Microwave properties of precipitation particles'. Quart. J. Roy. Meteor. Soc., Vol. 80, pp 522-545.

Haltiner, G. J., 1971. 'Numerical Weather Prediction'. John Wiley and Son, Inc., New York, 317 p. (See page 67).

Hoffer, R., E. G. Njoku, J. W. Waters, 1981. 'Microwave radiometer measurements of Sea surface temperature from Seasat Satellite: First results'. Science, Vol. 212, pp 1385-1387.

Holmstrom, I., 1963. 'On a method for parametric representation of the state of the atmosphere'. Tellus, Vol. 15, pp 127-149.

Jackson, J. D., 1962. 'Classical Electrodynamics'. Wiley (See p. 219).

Lane, J. A. and J. A. Saxton, 1952. 'Electrical properties of sea water'. Wireless Engineering, Vol. 29, pp. 269-275.

McClain, E. P., W. G. Pichel, C. C. Walton, Z. Ahmad and J. Sutton, 1982. 'Multichannel improvement to satellite derived sea surface temperatures'. Proceeding of XXIV COSPAR, Ottawa, Canada, May 1982, A.3., pp 1-11.

National Marine Fisheries Service Fishing Information. U.S. Dept. of Commerce, NOAA.

Njoku, E. G., 1980. 'Antenna pattern correction procedure for the scanning multichannel microwave radiometer (SMMR)'. Boundary Layer Meteorology, Vol. 18, pp 79-98.

Nordberg, W., J. Conaway, D. B. Ross, and T. Wilheit, 1971. 'Measurements of microwave emission from a foam-covered wind driven sea'. Jour. of Atm. Science, Vol. 38, pp 429-435.

Philips, N. A., 1956. 'The general circulation of the atmosphere: a numerical experiment'. Quart. Jour. Roy. Met. Soc., Vol. 82, pp 123-164.

Prabhakara, C., H. D. Chang, and A. T. C. Chang, 1982. 'Remote sensing of precipitable water over the oceans from Nimbus 7 microwave measurements'. Jour. Appl. Meteorology, Vol. 21, pp 59-68.

Prabhakara, C., G. Dalu, R. C. Lo and N. R. Nath, 1979. 'Remote sensing of seasonal distribution of precipitable water vapor over the oceans, and the inference of boundary-layer structure'. Monthly Weather Review, Vol. 107, pp 1388-1401.

Smith, W. L., and H. M. Woolf, 1976. 'The use of eigenvectors of statistical covariance matrices for interpreting satellite sounding radiometer observations'. Jour. of Atm. Sciences, Vol. 33, pp 1127-1140.

Staelin, D. H., K. F. Kunzi, R. L. Pettijohn, R. K. L. Poon, R. W. Wilcox, and J. W. Waters, 1976. 'Remote sensing of atmospheric water vapor and liquid water with Nimbus 5 microwave spectrometer'. Jour. of Appl. Meteor., Vol. 15, pp 1204-1214.

Swift, C. T., 1980. 'Passive Microwave remote sensing of ocean – A review'. Boundary Layer Meteorology, Vol. 18, pp 25-54.

Tsang, L., J. A. Kong, E. Njoku, D. H. Staelin, and J. W. Waters, 1977. 'Theory for microwave thermal emission from a layer of cloud or rain'. IEEE Transaction on Antennas and Propopogation, Ap-25(5), pp. 650-657.

Webster, W. J., T. T. Wilheit, D. B. Ross, and P. Gloersen, 1976. 'Spectral characteristics of the microwave emission from a wind driven foam-covered sea'. Jour. of Geophy. Res., Vol. 81, pp 3095-3099.

Wentz, F. J., 1981. 'Model function for ocean microwave brightness temperatures'. RSS Technical Report, Remote Sensing Systems. Sausalito, California, 58 p.

Wentz, F. J., 1982. 'Intercomparison of wind speeds inferred by the SASS. Altimeter and SMMR'. Jour. of Geophy. Res., Vol. 87, pp 3378-3384.

Wilheit, T. T., and A. T. C. Chang, 1980. 'An algorithm for retrieval of ocean surface and atmospheric parameters from the observations of the Scanning Multichannel Microwave Radiometer'. Radio Science, Vol. 15, pp 525-544.

Wilheit, T. T., 1979. 'A model for the microwave emissivity of the ocean's surface as a function of wind speed'. IEEE Transactions on Geoscience Electronics, Vol. G-E, No. 4, pp 244-249.

Wilheit, T. T., 1978. 'A review of applications of microwave radiometry to oceanography'. Boundary Layer Meteor., Vol. 13, pp 277-293.